

The Theory of Diffraction Tomography

Paul Müller¹, Mirjam Schürmann, and Jochen Guck
Biotechnology Center, Technische Universität Dresden, Dresden, Germany
(Dated: May 3, 2022)

Abstract

Tomography is the three-dimensional reconstruction of an object from images taken at different angles. The term classical tomography is used, when the imaging beam travels in straight lines through the object. This assumption is valid for light with short wavelengths, for example in x-ray tomography. For classical tomography, a commonly used reconstruction method is the filtered back-projection algorithm which yields fast and stable object reconstructions. In the context of single-cell imaging, the back-projection algorithm has been used to investigate the cell structure or to quantify the refractive index distribution within single cells using light from the visible spectrum. Nevertheless, these approaches, commonly summarized as optical projection tomography, do not take into account diffraction. Diffraction tomography with the Rytov approximation resolves this issue. The explicit incorporation of the wave nature of light results in an enhanced reconstruction of the object's refractive index distribution. Here, we present a full literature review of diffraction tomography. We derive the theory starting from the wave equation and discuss its validity with the focus on applications for refractive index tomography. Furthermore, we derive the back-propagation algorithm, the diffraction-tomographic pendant to the back-projection algorithm, and describe its implementation in three dimensions. Finally, we showcase the application of the back-propagation algorithm to computer-generated scattering data. This review unifies the different notations in literature and gives a detailed description of the back-propagation algorithm, serving as a reliable basis for future work in the field of diffraction tomography.

¹to whom correspondence should be addressed

Contents

Introduction	3
1 Tomography without Diffraction	4
1.1 Radon Transform	4
1.2 Fourier Slice Theorem	5
1.3 Backprojection Algorithm	6
2 The Wave Equation	8
2.1 Homogeneous Helmholtz Equation	8
2.2 Inhomogeneous Helmholtz Equation	9
3 Approximations to the Scattered Wave	10
3.1 Born Approximation	10
3.2 Rytov Approximation	12
4 Two-Dimensional Diffraction Tomography	16
4.1 Fourier Diffraction Theorem	16
4.2 Backpropagation Algorithm	20
5 Three-Dimensional Diffraction Tomography	24
5.1 Fourier Diffraction Theorem	25
5.2 Interpretation of the Fourier Diffraction Theorem	28
5.3 The Limes of the Rytov Approximation	30
5.4 Derivation with the Fourier Transform Approach	33
5.5 Backpropagation Algorithm	35
6 Implementation	43
6.1 Backprojection	44
6.2 Two-dimensional Backpropagation	45
6.3 Three-dimensional Backpropagation	47
Conclusions	48
A Notations in Literature	49
A.1 Two-dimensional Diffraction Tomography	49
A.2 Three-dimensional Diffraction Tomography	52
Bibliography	53
List of Figures and Tables	55
List of Symbols	56

Introduction

Computerized tomography (CT) is a common tool to image three-dimensional (3D) objects like e.g. bone tissue in the human body. The 3D object is reconstructed from transmission images at different angles, i.e. from projections onto a two-dimensional (2D) detector plane. The assumption that the recorded data are in fact projections is only valid for non-scattering objects, i.e. when the imaging beam travels in straight lines through the sample. A common technique to reconstruct the 3D object from 2D projections is the filtered backprojection algorithm. The term classical tomography is commonly used to identify reconstruction techniques that are based on this straight-line approach, neglecting diffraction.

When the wavelength of the imaging beam is large, i.e. comparable to the size of the imaged object, diffraction can not be neglected anymore and the assumptions of classical tomography are invalidated. The property that is responsible for diffraction at an object is its complex-valued refractive index distribution. The real part of the refractive index accounts for refraction of light and the imaginary part causes attenuation. Features in the refractive index distribution that are comparable in size to the wavelength of the light cause diffraction, i.e. the wavelike properties of light emerge. For example, organic tissue does not affect the directional propagation of x-ray radiation. Therefore, approximating the propagation of light in straight lines for CT is valid. However, small refractive index changes within single cells lead to diffraction of visible light, requiring a more fundamental model of light propagation. Diffraction tomography takes wave propagation into account (hence the name backpropagation algorithm) and can thus be applied to tomographic data sets that were imaged with large wavelengths. Therefore, diffraction tomography is ideally suited to resolve the refractive index of sub-cellular structures in single cells using light from the visible spectrum.

Because the refractive index distribution of single cells is mostly real-valued, they do not absorb significant amounts of light. Therefore, the main alteration of the wave front is due to refraction which is revealed by a measurable phase change. Therefore, diffraction tomography requires imaging techniques that quantify these sample-induced phase changes, such as digital holographic microscopy (DHM). The general problem is depicted in figure 1. For different angular positions,

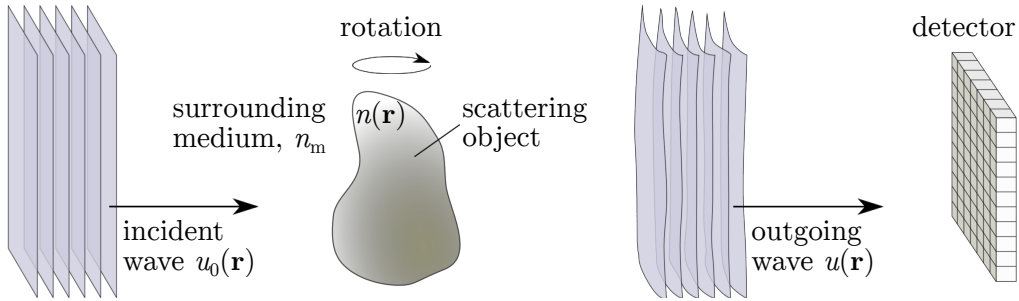


Figure 1, Tomographic data acquisition. An incident plane wave $u_0(\mathbf{r})$ is scattered by a transparent object with the refractive index distribution $n(\mathbf{r})$. A detector collects the scattered wave $u(\mathbf{r})$. Multi-angular acquisition is facilitated by rotation of the sample.

images of single-cell sized objects are recorded at the detector. A plane wave $u_0(\mathbf{r})$ with a wave-

length λ in the visible regime propagates through a biological cell with a certain real refractive index distribution $n(\mathbf{r})$. The recorded set of phase images, measured at different rotational positions of the cell, is called a sinogram. Sinograms are the starting point for the refractive index reconstruction in three dimensions.

The first section of the manuscript is a brief summary of non-diffraction tomographic methods. The two following sections introduce the wave equation and showcase the reconstruction from analytically computed sinograms. The subsequent chapters present the reconstruction algorithms [1–3] and their numerical implementation. The notation that we use here is similar to that used by the relevant literature (e.g. [4]). A list of symbols is given at the end of this manuscript.

1. Tomography without Diffraction

The first applications of computerized tomography (CT) used bone tissue as an inherent x-ray-absorbing marker. However, the marker can also be artificially introduced to the specimen. For example, in positron emission tomography (PET) radioactive tracers serve as markers for high metabolic activity. CT was also applied to biological specimens using wavelengths of the visible spectrum of light. The technique was termed optical projection tomography (OPT) [5]. In OPT, instead of measuring the absorption of the sample, the phase change introduced by the sample is measured. Thus, only the real part of the refractive index $n(\mathbf{r})$ is reconstructed, whereas in classical x-ray tomography the imaginary (absorbing) part of the refractive index is measured. In OPT, fluorescent markers can be used to complement the measurement of refractive index, just as PET does for classical x-ray CT. The algorithms presented in this section do not take into account the wave nature of light. They are only valid in the limit of small wavelengths, i.e. x-ray radiation or for very small refractive index variations $\epsilon_n(\mathbf{r}) = n(\mathbf{r}) - n_m$ of the sample $n(\mathbf{r})$ from the surrounding medium n_m .

1.1. Radon Transform

The Radon transform describes the forward tomographic process which is in general the projection of an n -dimensional function onto an $(n - 1)$ -dimensional plane. In the case of computerized tomography (CT), the forward process is the acquisition of two-dimensional (2D) projections from a three-dimensional (3D) volume². The 3D Radon transform can be described as a series of 2D Radon transforms for adjacent slices of the 3D volume. For the sake of simplicity, we consider only the two-dimensional case in the following derivations.

The value of one point in a projection is computed from the line integral through the detection volume [6]. The sample $f(\mathbf{r})$ is rotated through ϕ_0 along the y -axis. For each 2D slice of the sample $f(\mathbf{r})|_{y=y_s}$ at $y = y_s$, the one-dimensional projection $p_{\phi_0}(\mathbf{r}_D) = p_{\phi_0}(x_D, y_s)$ of this slice onto

²Keep in mind that in CT, the absorption of e.g. bone tissue is measured, whereas in optical tomography, the phase of the detected wave is measured.

a detector plane located at (x_D, y_s) is described by the Radon transform operator R_{ϕ_0} .

$$\begin{aligned} p_{\phi_0}(x_D, y_s) &= R_{\phi_0}\{f(\mathbf{r})|_{y=y_s}\}(x_D) \\ &= \int dv f(x(v), y_v, z(v)) \\ &= \int dv f(x_D \cos \phi_0 - v \sin \phi_0, y_s, x_D \sin \phi_0 + v \cos \phi_0) \end{aligned} \quad (1.1)$$

$$r_{xz}^2 = x^2 + z^2 = x_D^2 + v^2 \quad (1.2)$$

$$x_D = x \cos \phi_0 + z \sin \phi_0 \quad (1.3)$$

$$v = -x \sin \phi_0 + z \cos \phi_0 \quad (1.4)$$

Equation 1.2 defines a distance r_{xz} from the rotational center of the 2D slice. Equations 1.3 and 1.4 describe the dependency of the detector position at $x = x_D$ and the parameter v of the integral on the rotational position of the sample as defined by ϕ_0 . The equations are illustrated in figure 1.1.

Because the 3D Radon transform can be described by multiple 2D Radon transforms, the 3D reconstruction from a sinogram can also be described by multiple 2D reconstructions³.

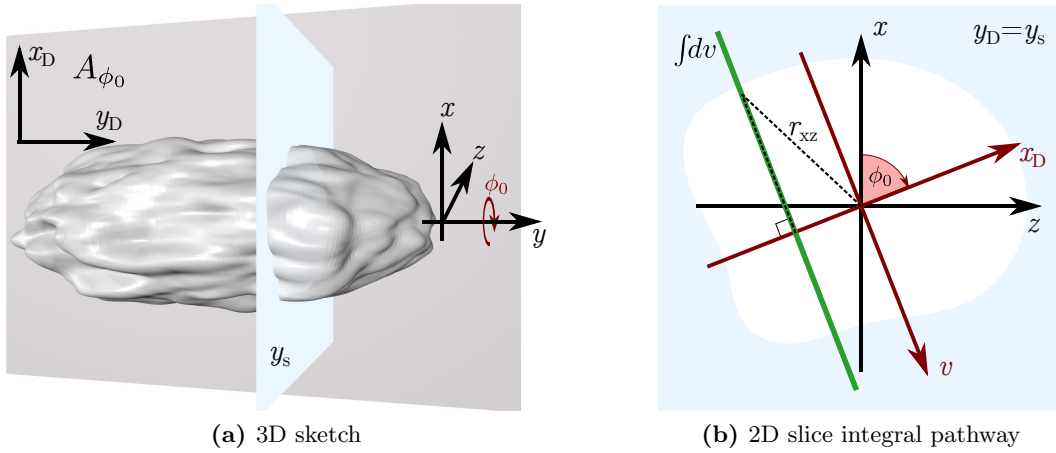


Figure 1.1, 3D Radon transform. **a)** Working principle of the three-dimensional (3D) Radon transform of a 3D object with the rotational axis y and the rotational angle ϕ_0 . For each slice of the object at y_s (blue plane), a two-dimensional Radon transform is performed. **b)** The two-dimensional Radon transform at y_s is computed by rotation of the object (white) through ϕ_0 (red coordinate system) and integration along v (green line) perpendicular to the detector line x_D .

1.2. Fourier Slice Theorem

The Fourier slice theorem is the central theorem in classical tomography. It connects the projection data $p_{\phi_0}(x_D)$ to the original image function $f(x, z)$ in Fourier space, which allows efficient reconstructions by means of the fast Fourier transform.

³This is not valid for diffraction tomography as discussed in sections 4 and 5.

The projection of a two-dimensional image $f(\mathbf{r})$ onto a detector line at an angle ϕ_0 can be written as the integral

$$p_{\phi_0}(x_D) = \int dv f(x(v), z(v)). \quad (1.1)$$

We define the unitary angular frequency Fourier transform of the one-dimensional data at the detector line with

$$\hat{P}_{\phi_0}(k_{Dx}) = \frac{1}{\sqrt{2\pi}} \int dx_D p_{\phi_0}(x_D) \exp(-ik_{Dx}x_D). \quad (1.5)$$

The actual Fourier transform $\hat{F}(\mathbf{k})$ of the two-dimensional image $f(\mathbf{r})$ is given by

$$\hat{F}(k_x, k_z) = \frac{1}{2\pi} \iint dx dz f(x, z) \exp(-i(k_x x + k_z z)). \quad (1.6)$$

This formula can be rewritten as (subscript ϕ_0 denotes rotation; the Jacobian of a rotation is 1)

$$\hat{F}_{\phi_0}(k_{Dx}, k_v) = \frac{1}{2\pi} \iint dx_D dv f_{\phi_0}(x_D, v) \exp(-i(k_{Dx}x_D + k_v v)) \quad (1.7)$$

$$f_{\phi_0}(x_D, v) = f(x_D \cos \phi_0 - v \sin \phi_0, x_D \sin \phi_0 + v \cos \phi_0) \quad (1.8)$$

$$\hat{F}_{\phi_0}(k_{Dx}, k_v) = F(k_{Dx} \cos \phi_0 - k_v \sin \phi_0, k_{Dx} \sin \phi_0 + k_v \cos \phi_0). \quad (1.9)$$

For the case $k_v = 0$ (which implies slicing $\hat{F}(\mathbf{k})$ at the angle ϕ_0), we arrive at [7–9]

$$\hat{F}_{\phi_0}(k_{Dx}, 0) = \frac{1}{\sqrt{2\pi}} \hat{P}_{\phi_0}(k_{Dx}). \quad (1.10)$$

This formula, known as the Fourier slice theorem, states that the Fourier transform of a projection at an angle ϕ_0 is distributed along a straight line at the same angle in the Fourier space of the image $f(\mathbf{r})$. This theorem allows us to compute the inverse of the Radon transform operator R_{ϕ_0} by interpolating $\hat{F}(\mathbf{k})$ from $\hat{P}_{\phi_0}(k_{Dx})$ in Fourier space and subsequently performing an inverse Fourier transform.

In order to compute the inverse Radon transform in Fourier space, we have to interpolate the data in Fourier space on a rectangular grid. However, this technique is afflicted with interpolation artifacts. Alternatively, one often uses the backprojection algorithm which is introduced in the next section.

1.3. Backprojection Algorithm

The backprojection algorithm connects the object function $f(x, z)$ to the Fourier transform of the projection $\hat{P}_{\phi_0}(k_{Dx})$. In order to derive it, we first express the object function $f(x, z)$ as the inverse Fourier transform of $\hat{F}(\mathbf{k})$.

$$f(x, z) = \frac{1}{2\pi} \iint dk_x dk_z \hat{F}(k_x, k_z) \exp(i(k_x x + k_z z)) \quad (1.11)$$

We then perform a coordinate transform from (k_x, k_z) to (k_{Dx}, ϕ_0) . It can be easily shown that the Jacobian computes to

$$\left| \det \left(\frac{d(k_x, k_z)}{d(k_{Dx}, \phi_0)} \right) \right| = |k_{Dx}|. \quad (1.12)$$

$$k_x = k_{Dx} \cos \phi_0 - k_v \sin \phi_0 \quad (1.13)$$

$$k_z = k_{Dx} \sin \phi_0 + k_v \cos \phi_0 \quad (1.14)$$

$$k_v = 0 \quad (1.15)$$

Therefore, combining equations 1.10 to 1.15, we get [7–11]

$$f(x, z) = \frac{1}{2\pi} \int dk_{Dx} \int_0^\pi d\phi_0 |k_{Dx}| \frac{\hat{P}_{\phi_0}(k_{Dx})}{\sqrt{2\pi}} \exp[ik_{Dx}(x \cos \phi_0 + z \sin \phi_0)]. \quad (1.16)$$

Note that the integral over ϕ_0 runs from 0 to π . The integrals of k_x , k_z , and k_{Dx} are computed over the entire k -space, i.e. over the interval $(-\infty, +\infty)$. The term $|k_{Dx}|$ is a ramp filter in Fourier space which lead to the common term *filtered* backprojection algorithm in literature. However, we refer to it as the backprojection algorithm throughout this manuscript.

Figure 1.2 depicts the sinogram acquisition and image reconstruction of a two-dimensional test target with the backprojection algorithm from 30 and 100 angular projections. Note that because of our chosen coordinate system, at the angle $\phi_0 = 0$, k_{Dx} coincides with the k_x axis ($x_D \stackrel{\phi_0=0}{=} x$).

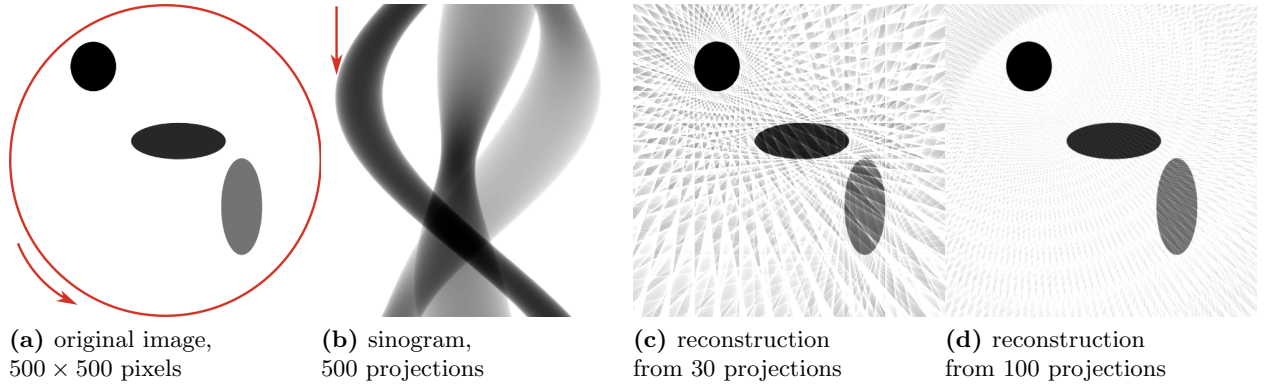


Figure 1.2, Backprojection. **a)** The original two-dimensional image contains ellipses of different gray-scale levels. **b)** The sinogram shows 500 projection of image (a) from 0° to 180° . For the computation of the sinogram, only the circular region of the original image (red) was used. **c)** Reconstruction using 30 equidistant projections. **d)** Reconstruction with 100 projections. The sinogram and reconstructions were created with the Python library radon [12].

As discussed in the introduction, the backprojection algorithm assumes that light propagates along straight lines. It is thus not an optimal method for optical tomography which employs wavelengths that are in the visible spectrum of light. Thus, we need to include the wave nature of light in our reconstruction scheme. The next two chapters introduce the foundation of the Fourier diffraction theorem which yields better reconstruction results for objects that diffract light.

2. The Wave Equation

The propagation of light through objects in space \mathbf{r} and time t follows the Maxwell equations. Light propagation through empty space can be described by the wave equation, which simplifies the vectorial description of electromagnetic fields to a scalar description of waves. When light propagates through inhomogeneous media, the wave equation does not anymore provide an exact description because the vectorial components of the electromagnetic field couple at e.g. refractive index boundaries. However, it is known that the wave equation is a good approximation for light propagation in inhomogeneous media [13] and we show that this scalar approximation of vectorial fields is valid for the discussed test targets. The wave equation reads

$$\frac{\partial^2}{\partial t^2} \Psi(\mathbf{r}, t) = \left(\frac{c_0}{n(\mathbf{r})} \right)^2 \cdot \nabla^2 \Psi(\mathbf{r}, t), \quad (2.1)$$

where $\Psi(\mathbf{r}, t)$ is a time-dependent, scalar wave field in space, c_0 is the speed of light in vacuum, and $n(\mathbf{r})$ is the spatial refractive index distribution. Note that $\frac{c_0}{n(\mathbf{r})}$ is usually a constant coefficient which describes the speed of the propagating wave. Because we are not interested in the temporal information of $\Psi(\mathbf{r}, t)$, we may simplify the wave equation by separation of variables. We then obtain the time-independent wave equation, known as the Helmholtz equation [14]

$$(\nabla^2 + k(\mathbf{r})^2) u(\mathbf{r}) = 0, \quad (2.2)$$

where $k(\mathbf{r})$ is the wave number that depends on the local refractive index distribution $n(\mathbf{r})$ and $u(\mathbf{r})$ is the scattered field. To simplify the notation, we introduce the wave number inside the medium surrounding a sample k_m and the local variation in refractive index inside a sample $\epsilon_n(\mathbf{r})$ as follows,

$$k_m = \frac{2\pi n_m}{\lambda} \quad (2.3)$$

$$n(\mathbf{r}) = n_m + \epsilon_n(\mathbf{r}) \quad (2.4)$$

$$\begin{aligned} k(\mathbf{r}) &= k_m \frac{n(\mathbf{r})}{n_m} \\ &= k_m \left(1 + \frac{\epsilon_n(\mathbf{r})}{n_m} \right) \end{aligned} \quad (2.5)$$

where λ is the vacuum wavelength of the light.

2.1. Homogeneous Helmholtz Equation

For the homogeneous case, i.e. there is no sample ($\epsilon_n(\mathbf{r}) = 0$), the wave equation becomes the Helmholtz equation for a homogeneous medium

$$(\nabla^2 + k_m^2) u_0(\mathbf{r}) = 0. \quad (2.6)$$

This second order ordinary differential equation has plane wave solutions of the form

$$u_0(\mathbf{r}) = a_0 \exp(ik_m \mathbf{s}_0 \cdot \mathbf{r}), \quad (2.7)$$

where \mathbf{s}_0 is the normal unit vector and a_0 is the amplitude of the plane wave. Throughout this script, we use the convention that $u_0(\mathbf{r})$ in equation 2.7 defines a wave traveling from left to right, and thus $u_0(\mathbf{r})$ has a '+'-sign in the exponent. This convention is widely used in the literature dealing with diffraction tomography [1, 3, 4].

2.2. Inhomogeneous Helmholtz Equation

Equation 2.2 can be rewritten as the inhomogeneous Helmholtz equation

$$(\nabla^2 + k_m^2) u(\mathbf{r}) = -f(\mathbf{r}) u(\mathbf{r}) \quad (2.8)$$

$$\text{with } f(\mathbf{r}) = k_m^2 \left[\left(\frac{n(\mathbf{r})}{n_m} \right)^2 - 1 \right]. \quad (2.9)$$

In order to deal with the inhomogeneity $f(\mathbf{r})$, we can make use of the Green's function $G(\mathbf{r} - \mathbf{r}')$ that is defined by equation 2.10⁴. The Green's function for the homogeneous Helmholtz equation is shown in equation 2.11⁵.

$$(\nabla^2 + k_m^2) G(\mathbf{r} - \mathbf{r}') = -\delta(\mathbf{r} - \mathbf{r}') \quad (2.10)$$

$$G(\mathbf{r} - \mathbf{r}') = \frac{\exp(ik_m |\mathbf{r} - \mathbf{r}'|)}{4\pi |\mathbf{r} - \mathbf{r}'|} \quad (2.11)$$

Here, $\delta(\mathbf{r} - \mathbf{r}')$ is the Dirac delta function with the translational property

$$\int d^3 r' \delta(\mathbf{r} - \mathbf{r}') g(\mathbf{r}') = g(\mathbf{r}). \quad (2.12)$$

By knowledge of the Green's function we can derive an integral representation for the scattered field $u(\mathbf{r})$. Using equation 2.12, the right side of equation 2.8 can be integrated to include the Green's function (eq. 2.10)⁶

$$f(\mathbf{r}) u(\mathbf{r}) = \int d^3 r' \delta(\mathbf{r} - \mathbf{r}') f(\mathbf{r}') u(\mathbf{r}') \quad (2.13)$$

$$= - \int d^3 r' (\nabla^2 + k_m^2) G(\mathbf{r} - \mathbf{r}') f(\mathbf{r}') u(\mathbf{r}') \quad (2.14)$$

$$= - (\nabla^2 + k_m^2) \int d^3 r' G(\mathbf{r} - \mathbf{r}') f(\mathbf{r}') u(\mathbf{r}'). \quad (2.15)$$

The comparison of equations 2.8 and 2.15 suggests that the scattered field $u(\mathbf{r})$ can be written as

$$u(\mathbf{r}) = \int d^3 r' G(\mathbf{r} - \mathbf{r}') f(\mathbf{r}') u(\mathbf{r}') \quad (2.16)$$

which is the integral equation to the inhomogeneous wave equation (eq. 2.8).

⁴The Green's function is defined as the solution to the inhomogeneous problem: When the operator $(\nabla^2 + k_m^2)$ is applied to $G(\mathbf{r} - \mathbf{r}')$, one obtains the Dirac delta distribution $\delta(\mathbf{r} - \mathbf{r}')$.

⁵Note that our notation implies the (+)-sign and a normalization factor of 4π for the Green's function. For a derivation see for example [15], section 2.4 or [16], section 7.2.

⁶Note that the Green's function depends on the absolute value of $|\mathbf{r} - \mathbf{r}'|$ and thus $(\nabla'^2 + k_m^2) G(\mathbf{r} - \mathbf{r}') = (\nabla^2 + k_m^2) G(\mathbf{r} - \mathbf{r}')$

3. Approximations to the Scattered Wave

Equation 2.16 has no analytical solution. However, under certain conditions approximations can be applied to find a solution. In this section, we derive the Born and Rytov approximations. Both approximations define the scattered field $u(\mathbf{r})$ as a superposition of the incident plane wave $u_0(\mathbf{r})$ and a scattered component $u_s(\mathbf{r})$.

$$u(\mathbf{r}) = u_0(\mathbf{r}) + u_s(\mathbf{r}) \quad (3.1)$$

3.1. Born Approximation

The Born approximation uses the property of the homogeneous component

$$(\nabla^2 + k_m^2) u_0(\mathbf{r}) = 0 \quad (3.2)$$

to rewrite the inhomogeneous wave equation for the scattered component $u_s(\mathbf{r})$

$$(\nabla^2 + k_m^2) u(\mathbf{r}) = (\nabla^2 + k_m^2) u_s(\mathbf{r}) = -f(\mathbf{r})u(\mathbf{r}). \quad (3.3)$$

By once again using the translational property of the delta function (eq. 2.12) we obtain an iterative equation for $u_s(\mathbf{r})$

$$u_s(\mathbf{r}) = \int d^3r' G(\mathbf{r} - \mathbf{r}') f(\mathbf{r}') u(\mathbf{r}') \quad (3.4)$$

and we can write the Lippmann-Schwinger equation for the field $u(\mathbf{r})$ with the perturbation $f(\mathbf{r})$ [14]

$$u(\mathbf{r}) = u_0(\mathbf{r}) + \int d^3r' G(\mathbf{r} - \mathbf{r}') f(\mathbf{r}') u(\mathbf{r}'). \quad (3.5)$$

By iteratively replacing $u(\mathbf{r})$ in the above integral, one obtains the Born series. The Born approximation is actually the first iteration of the Born series [14].

$$u(\mathbf{r}) \stackrel{\text{Born}}{\approx} u_0(\mathbf{r}) + u_B(\mathbf{r}) \quad (3.6)$$

$$u_B(\mathbf{r}) = \int d^3r' G(\mathbf{r} - \mathbf{r}') f(\mathbf{r}') u_0(\mathbf{r}'). \quad (3.7)$$

Validity of the Born Approximation

In the derivation above, approximating the scattered component $u_s(\mathbf{r})$ as the first term of the Born series $u_B(\mathbf{r})$ implies that

$$\int d^3r' G(\mathbf{r} - \mathbf{r}') f(\mathbf{r}') [u_0(\mathbf{r}') + u_s(\mathbf{r}')] \approx \int d^3r' G(\mathbf{r} - \mathbf{r}') f(\mathbf{r}') u_0(\mathbf{r}') \quad (3.8)$$

$$\text{or } u_0(\mathbf{r}) + u_s(\mathbf{r}) \approx u_0(\mathbf{r}).$$

Thus, the Born approximation holds for the case “ $u_s(\mathbf{r}) \ll u_0(\mathbf{r})$ ”, i.e. the contributions of amplitude and phase of the scattering component $u_s(\mathbf{r})$ are small when compared to the incident plane

wave $u_0(\mathbf{r})$. Since both $u_s(\mathbf{r})$ and $u_0(\mathbf{r})$ are complex-valued functions, the above relation implies that (i) there is only little absorption by the specimen and that (ii) the overall phase change $\Delta\Phi$ must be small. Because we are interested in biological cells whose imaginary part of the refractive index is insignificant, (i) absorption is negligible and we thus focus on (ii) the phase change $\Delta\Phi$ introduced by the cell. The phase change $\Delta\Phi$ that a scattered wave $u_s(\mathbf{r})$ experiences when traveling through a sample along a certain path parametrized by s_{path} can be approximated with ray optics

$$\Delta\Phi \approx \frac{2\pi}{\lambda} \left(\int_{\text{path}} ds_{\text{path}} n(\mathbf{r}) - s_{\text{tot}} n_{\text{m}} \right), \quad (3.9)$$

where $n(\mathbf{r})$ is the refractive index distribution inside the sample, s is the approximate thickness of the sample, and n_{m} is the refractive index of the medium surrounding the sample. For a homogeneous sample with the refractive index n_{s} , the absolute phase change computes to

$$\Delta\Phi = \frac{2\pi}{\lambda} s(n_{\text{s}} - n_{\text{m}}) = \frac{2\pi}{\lambda} s\epsilon_{\text{n}}. \quad (3.10)$$

This equation can be interpreted as a comparison of the phase change $\Delta\Phi$ over a period of 2π with the change of the optical path length $s(n_{\text{s}} - n_{\text{m}})$ over one wavelength λ .

We now want to write equation 3.10 in its differential form. We express the total differential of $\Delta\Phi$ with respect to the spatial distance s and the refractive index variation ϵ_{n} as

$$\frac{d(\Delta\Phi)}{2\pi} = \frac{\epsilon_{\text{n}}}{\lambda} ds + \frac{s}{\lambda} d\epsilon_{\text{n}}. \quad (3.11)$$

The phase change $\Delta\Phi$ can have two contributions, namely the thickness of the sample

$$\frac{d(\Delta\Phi_{\text{A}})}{2\pi} = \frac{\epsilon_{\text{n}}}{\lambda} ds \quad (3.12)$$

and the refractive index variation inside the sample

$$\frac{d(\Delta\Phi_{\text{B}})}{2\pi} = \frac{s}{\lambda} d\epsilon_{\text{n}}. \quad (3.13)$$

Note that in general ϵ_{n} is dependent on \mathbf{r} (3D) and that $\Delta\Phi$ is measured at the detector plane \mathbf{r}_{D} (2D). If the refractive index of the sample is fixed, then the total phase change solely depends on the thickness of the sample. If the thickness of the sample is fixed, the local variations inside the sample determine the absolute phase change. If we wanted to consider a phase change that is introduced by a refractive index variation over the distance of one wavelength λ , then we would have to set $s = \lambda$.

With these considerations, we can answer the question of the validity of the Born approximation. We interpret the inequality “ $u_{\text{s}}(\mathbf{r}) \ll u_0(\mathbf{r})$ ” as a general restriction: The overall phase change must be much smaller than 2π . According to equation 3.10, this translates to a restriction for the

optical path difference $s(n_s - n_m)$ which must be much smaller than the wavelength λ of the used light

$$\Delta\Phi \ll 2\pi \quad (3.14)$$

$$s(n_s - n_m) \ll \lambda. \quad (3.15)$$

The fact that the Born approximation only allows to observe optically thin samples is a serious drawback. A second approach to the problem is the Rytov approximation.

3.2. Rytov Approximation

In order to derive the Rytov approximation we assume that the scattered wave $u(\mathbf{r})$ and the incident wave $u_0(\mathbf{r})$ have the form

$$u(\mathbf{r}) = \exp(\varphi(\mathbf{r})) = u_0(\mathbf{r}) + u_s(\mathbf{r}) \quad (3.16)$$

$$u_0(\mathbf{r}) = \exp(\varphi_0(\mathbf{r})) \quad (3.17)$$

$$\varphi(\mathbf{r}) = \varphi_0(\mathbf{r}) + \varphi_s(\mathbf{r}) \quad (3.18)$$

where we use the complex phases

$$\varphi(\mathbf{r}) = i\Phi(\mathbf{r}) + \ln(a(\mathbf{r})) \quad (3.19)$$

$$\varphi_0(\mathbf{r}) = i\Phi_0(\mathbf{r}) + \ln(a_0(\mathbf{r})) \quad (3.20)$$

to denote the complex exponent containing phase and amplitude of the wave function. Note that $u_s(\mathbf{r})$ is now computed from $\varphi_s(\mathbf{r})$ with

$$u_s(\mathbf{r}) = u(\mathbf{r}) - u_0(\mathbf{r}) \quad (3.21)$$

$$= \exp(\varphi_0(\mathbf{r})) [\exp(\varphi_s(\mathbf{r})) - 1]. \quad (3.22)$$

Using the equations above, the inhomogeneous wave equation becomes

$$(\nabla^2 + k_m^2)u(\mathbf{r}) = -f(\mathbf{r})u(\mathbf{r}) \quad (3.23)$$

$$(\nabla^2 + k_m^2)\exp(\varphi(\mathbf{r})) = -f(\mathbf{r})\exp(\varphi(\mathbf{r})). \quad (3.24)$$

We can then compute the term $\nabla^2 \exp(\varphi(\mathbf{r}))$

$$\nabla^2 \exp(\varphi(\mathbf{r})) = \nabla [\exp(\varphi(\mathbf{r})) \cdot \nabla \varphi(\mathbf{r})] \quad (3.25)$$

$$\nabla^2 \exp(\varphi(\mathbf{r})) = \exp(\varphi(\mathbf{r})) [\nabla^2 \varphi(\mathbf{r}) + (\nabla \varphi(\mathbf{r}))^2] \quad (3.26)$$

to obtain a differential equation for $\varphi(\mathbf{r})$.

$$\exp(\varphi(\mathbf{r})) [\nabla^2 \varphi(\mathbf{r}) + (\nabla \varphi(\mathbf{r}))^2 + k_m^2] = -f(\mathbf{r})\exp(\varphi(\mathbf{r})) \quad (3.27)$$

$$\nabla^2 \varphi(\mathbf{r}) + (\nabla \varphi(\mathbf{r}))^2 + k_m^2 = -f(\mathbf{r}) \quad (3.28)$$

Equation 3.28 is a non-linear differential equation for the complex phase $\varphi(\mathbf{r})$. In the same manner, a differential equation for $\varphi_0(\mathbf{r})$ can be derived

$$\nabla^2 \varphi_0(\mathbf{r}) + (\nabla \varphi_0(\mathbf{r}))^2 + k_m^2 = 0. \quad (3.29)$$

The next step is to insert equation 3.18 into equation 3.28 to find a differential equation for $\varphi_s(\mathbf{r})$.

$$\nabla^2 [\underline{\varphi_0(\mathbf{r})} + \varphi_s(\mathbf{r})] + \frac{(\nabla [\varphi_0(\mathbf{r}) + \varphi_s(\mathbf{r})])^2}{(\nabla \varphi_0(\mathbf{r}))^2 + 2\nabla \varphi_0(\mathbf{r}) \cdot \nabla \varphi_s(\mathbf{r}) + (\nabla \varphi_s(\mathbf{r}))^2} + \underline{k_m^2} = -f(\mathbf{r}) \quad (3.30)$$

The terms marked with an underline compute to zero (eq. 3.29) and the equation above becomes

$$\nabla^2 \varphi_s(\mathbf{r}) + 2\nabla \varphi_s(\mathbf{r}) \cdot \nabla \varphi_0(\mathbf{r}) + (\nabla \varphi_s(\mathbf{r}))^2 = -f(\mathbf{r}). \quad (3.31)$$

To simplify this expression we need to consider

$$\nabla^2 u_0(\mathbf{r}) \varphi_s(\mathbf{r}) = \underbrace{\nabla^2 u_0(\mathbf{r}) \cdot \varphi_s(\mathbf{r})}_{-k_m^2 u_0(\mathbf{r})} + 2 \underbrace{\nabla u_0(\mathbf{r}) \cdot \nabla \varphi_s(\mathbf{r})}_{u_0(\mathbf{r}) \nabla \varphi_0(\mathbf{r})} + u_0(\mathbf{r}) \nabla^2 \varphi_s(\mathbf{r}). \quad (3.32)$$

$$\downarrow$$

$$(\nabla^2 + k_m^2) u_0(\mathbf{r}) \varphi_s(\mathbf{r}) = 2u_0(\mathbf{r}) \nabla \varphi_0(\mathbf{r}) \cdot \nabla \varphi_s(\mathbf{r}) + u_0(\mathbf{r}) \nabla^2 \varphi_s(\mathbf{r}) \quad (3.33)$$

If we multiply equation 3.31 by $u_0(\mathbf{r})$ then we can substitute with equation 3.33 to obtain

$$(\nabla^2 + k_m^2) u_0(\mathbf{r}) \underbrace{\varphi_s(\mathbf{r})}_{\underset{\text{Rytov}}{\approx} \varphi_R(\mathbf{r})} = -u_0(\mathbf{r}) \underbrace{[(\nabla \varphi_s(\mathbf{r}))^2 + f(\mathbf{r})]}_{\underset{\text{Rytov}}{\approx} f(\mathbf{r})}. \quad (3.34)$$

The Rytov approximation assumes that the phase gradient $\nabla \varphi_s(\mathbf{r})$ is small compared to the perturbation $f(\mathbf{r})$. We can now make use of the Green's function again (eqns. 2.10 to 2.16) and arrive at the formula for the Rytov Phase $\varphi_R(\mathbf{r})$ [4].

$$u_0(\mathbf{r}) \varphi_R(\mathbf{r}) = \int d^3 r' G(\mathbf{r} - \mathbf{r}') f(\mathbf{r}') u_0(\mathbf{r}') \quad (3.35)$$

$$\varphi_R(\mathbf{r}) = \frac{\int d^3 r' G(\mathbf{r} - \mathbf{r}') f(\mathbf{r}') u_0(\mathbf{r}')}{u_0(\mathbf{r})} \quad (3.36)$$

By comparing this expression to the first Born approximation (eq. 3.6) we find that we can compute the Rytov approximation $u_R(\mathbf{r})$ from the Born approximation $u_B(\mathbf{r})$ and vice versa.

$$\varphi_R(\mathbf{r}) = \frac{u_B(\mathbf{r})}{u_0(\mathbf{r})} \quad (3.37)$$

$$u_R(\mathbf{r}) = u_0(\mathbf{r}) \left[\exp\left(\frac{u_B(\mathbf{r})}{u_0(\mathbf{r})}\right) - 1 \right] \quad (3.38)$$

$$u_B(\mathbf{r}) = u_0(\mathbf{r}) \ln\left(\frac{u_R(\mathbf{r})}{u_0(\mathbf{r})} + 1\right) \quad (3.39)$$

$$= u_0(\mathbf{r}) \varphi_R(\mathbf{r}) \quad (3.40)$$

$$u(\mathbf{r}) \stackrel{\text{Born}}{\approx} u_0(\mathbf{r}) + u_B(\mathbf{r})$$

$$u(\mathbf{r}) \stackrel{\text{Rytov}}{\approx} u_0(\mathbf{r}) + u_R(\mathbf{r})$$

Note that the complex Rytov phase $\varphi_R(\mathbf{r})$ also contains the amplitude information of the scattered wave. In section 5.5 we introduce a backpropagation algorithm for the Born approximation. This algorithm may also be used in combination with the Rytov approximation by using equation 3.39. In practice, calculating the logarithm of $\exp(\varphi(\mathbf{r}) - \varphi_0(\mathbf{r}))$ involves calculating the logarithm of the amplitudes and the phases.

$$\ln(\exp(\varphi(\mathbf{r}) - \varphi_0(\mathbf{r}))) = \ln\left(\frac{a(\mathbf{r})}{a_0(\mathbf{r})}\right) + i(\Phi(\mathbf{r}) - \Phi_0(\mathbf{r})) \quad (3.41)$$

Because the phase $\Phi(\mathbf{r}) - \Phi_0(\mathbf{r})$ is modulo 2π , a computational implementation of the Rytov approximation must contain a phase-unwrapping algorithm [17].

Validity of the Rytov Approximation

From our approximation in equation 3.34, we can tell that the Rytov approximation is valid for the case

$$\begin{aligned} (\nabla \varphi_s(\mathbf{r}))^2 &\ll f(\mathbf{r}) \\ &\stackrel{\text{eq. 2.9}}{\ll} k_m^2 \left[\left(\frac{n(\mathbf{r})}{n_m} \right)^2 - 1 \right] \end{aligned} \quad (3.42)$$

$$n(\mathbf{r})^2 \gg n_m^2 \left[\frac{(\nabla \varphi_s(\mathbf{r}))^2}{k_m^2} + 1 \right]. \quad (3.43)$$

We are interested in a validity condition that connects the refractive index with its gradient. We insert the definitions of the wave vector k_m and the refractive index distribution $n(\mathbf{r})$ (eq. 2.3, 2.4)

to retrieve a condition for the variation in refractive index $\epsilon_n(\mathbf{r})$.

$$n(\mathbf{r})^2 \gg n_m^2 \left(\frac{\nabla \varphi_s(\mathbf{r}) \lambda}{2\pi n_m} \right)^2 + n_m^2 \quad (3.44)$$

$$n(\mathbf{r})^2 - n_m^2 \gg \left(\frac{\nabla \varphi_s(\mathbf{r}) \lambda}{2\pi} \right)^2 \quad (3.45)$$

$$\underbrace{\epsilon_n(\mathbf{r})^2}_{\approx 0} + 2n_m \epsilon_n(\mathbf{r}) \gg \left(\frac{\nabla \varphi_s(\mathbf{r}) \lambda}{2\pi} \right)^2 \quad (3.46)$$

Because the local variation $\epsilon_n(\mathbf{r})$ is small, we may neglect⁷ $\epsilon_n(\mathbf{r})^2$. The resulting constraint for the phase gradient is [4]

$$\frac{|\nabla \varphi_s(\mathbf{r})|}{2\pi} \ll \frac{\sqrt{2n_m |\epsilon_n(\mathbf{r})|}}{\lambda} \quad (3.47)$$

$$\frac{|d\varphi_s(\mathbf{r})|}{2\pi} \ll \frac{\sqrt{2n_m |\epsilon_n(\mathbf{r})|} \cdot |d\mathbf{r}|}{\lambda}. \quad (3.48)$$

For any position \mathbf{r} inside a sample, equation 3.48 reads:

The sample induces a phase change over a period of 2π radians. This number must be smaller than the variation in refractive index $\epsilon_n(\mathbf{r})$ along the corresponding optical path scaled by the used wavelength λ .

Note that the total phase gradient is computed from

$$|\nabla \varphi(\mathbf{r})| = |\nabla \varphi_0(\mathbf{r}) + \nabla \varphi_s(\mathbf{r})| \quad (3.49)$$

$$|\nabla \varphi(\mathbf{r})| = |i\mathbf{k}_m + \nabla \varphi_s(\mathbf{r})|. \quad (3.50)$$

Thus, compared to the Born approximation, where the overall phase change must be smaller than 2π , the Rytov approximation is also valid for thicker samples. The Rytov approximation is accurate for small wavelengths and breaks down for large variations in the refractive index [18]. When we insert equation 3.13 into equation 3.48 ($\Delta\Phi_B = \varphi_s(\mathbf{r})$), we obtain the restriction for the Rytov approximation.

$$\frac{d\epsilon_n(\mathbf{r})}{|d\mathbf{r}|} \ll \frac{\sqrt{2n_m |\epsilon_n(\mathbf{r})|}}{\lambda} \quad (3.51)$$

We set $s = \lambda$, because we know that in equation 3.48 the total path length that leads to a phase change for $\varphi_s(\mathbf{r})$ is λ and in equation 3.13 this path length is s . The term $d\epsilon_n(\mathbf{r})/|d\mathbf{r}|$ can be thought of as the gradient of $\epsilon_n(\mathbf{r})$.

$$|\nabla n(\mathbf{r})| \ll \frac{\sqrt{2n_m |n(\mathbf{r}) - n_m|}}{\lambda} \quad (3.52)$$

The validity of the Rytov approximation is not dependent on the absolute phase change introduced by the sample, but on the gradient of the refractive index within the sample. This makes the Rytov approximation applicable to biological cells. The application of the Rytov approximation to the three-dimensional backpropagation algorithms is described in section 5.3.

⁷This can be shown by solving the quadratic equation 3.46 for $\epsilon_n(\mathbf{r})$ and Taylor-expanding for small $\nabla \varphi_s(\mathbf{r})$ to the second order.

4. Two-Dimensional Diffraction Tomography

The name *Fourier diffraction theorem* was introduced by Slaney and Kak [4] in the 1980's. In the limit of small wavelengths, the Fourier diffraction theorem in the Rytov approximation converges to the Fourier slice theorem (section 5.3, [2]). In this section, we derive the two-dimensional backpropagation algorithm, as described by Kak and Slaney [4], which was implemented in the C programming language in 1988⁸. At the end of the section, we test the backpropagation algorithm with artificial data that were computed using Mie theory. Mie theory provides solutions to the Maxwell equations in the form of infinite series for scattering objects consisting of simple geometric shapes. It is thus ideally suited to test the approximations made in sections 2 and 3. The 3D theory can be derived analogous to the 2D theory. It is described and discussed in greater detail in section 5. Throughout this section we use two-dimensional vectors, i.e. $\mathbf{r} = (x, z)$.

4.1. Fourier Diffraction Theorem

We start from the inhomogeneous wave equation as discussed in section 2.2.

$$(\nabla^2 + k_m^2) u(\mathbf{r}) = -\delta(\mathbf{r} - \mathbf{r}') \quad (4.1)$$

The Green's function in the two-dimensional case is the zero-order Hankel function of the first kind.

$$G(\mathbf{r} - \mathbf{r}') = \frac{\exp(ik_m |\mathbf{r} - \mathbf{r}'|)}{4\pi |\mathbf{r} - \mathbf{r}'|} \quad (4.2)$$

$$= \frac{i}{4} H_0^{(1)}(k_m |\mathbf{r} - \mathbf{r}'|) \quad (4.3)$$

$$H_0^{(1)}(k_m |\mathbf{r} - \mathbf{r}'|) = \frac{1}{\pi} \int dk_x \frac{1}{\gamma} \exp\{i [k_x(x - x') + \gamma(z - z')]\} \quad (4.4)$$

$$\gamma = \sqrt{k_m^2 - k_x^2} \quad (4.5)$$

We observe restrictions for the Cartesian coordinates for the vector \mathbf{s}_0 describing the incoming plane wave and the vector \mathbf{s} describing an arbitrarily scattered wave. The following substitutions are defined by our notation:

$$k_x = k_m p, \quad \gamma = k_m M \quad (4.6)$$

$$M = \sqrt{1 - p^2}, \quad M_0 = \sqrt{1 - p_0^2} \quad (4.7)$$

$$\mathbf{s} = (p, M), \quad \mathbf{s}_0 = (p_0, M_0) \quad (4.8)$$

The parameters p and p_0 describe the k_x -component of the vectors \mathbf{s} and \mathbf{s}_0 . They must fulfill the relation $0 \leq p, p_0 \leq 1$. In order to have the data consistent with section 1 (Fourier slice theorem), \mathbf{s}_0 points into the z -direction when $\phi_0 = 0$. This means that $\mathbf{s}_0 = (-\sin \phi_0, \cos \phi_0)$. We rewrite the Green's function accordingly.

$$G(\mathbf{r} - \mathbf{r}') = \frac{i}{4\pi} \int dp \frac{1}{M} \exp\{ik_m [p(x - x') + M(z - z')]\} \quad (4.9)$$

⁸implemented by Malcolm Slaney, available at <http://slaney.org>; see also [19]

In our notation, the incoming plane wave $u_0(\mathbf{r})$ with amplitude a_0 , propagation direction \mathbf{s}_0 , and wavenumber k_m can be written as

$$u_0(\mathbf{r}) = a_0 \exp(ik_m \mathbf{s}_0 \mathbf{r}). \quad (4.10)$$

The first Born approximation in two dimensions then reads (see section 3.1).

$$u_B(\mathbf{r}) = \iint d^2 r' G(\mathbf{r} - \mathbf{r}') f(\mathbf{r}') u_0(\mathbf{r}') \quad (4.11)$$

We define the two-dimensional Fourier transform $\hat{F}(\mathbf{k})$ of the object function $f(\mathbf{r})$

$$\hat{F}(\mathbf{k}) = \frac{1}{2\pi} \iint d^2 r f(\mathbf{r}) \exp(-i\mathbf{k}\mathbf{r}) \quad (4.12)$$

$$f(\mathbf{r}) = \frac{1}{2\pi} \iint d^2 k \hat{F}(\mathbf{k}) \exp(i\mathbf{k}\mathbf{r}) \quad (4.13)$$

and we keep in mind the identity of the Dirac delta distribution for any given p and a

$$\delta(p - a) = \frac{1}{2\pi} \int dx \exp(i(p - a)x). \quad (4.14)$$

We now insert equation 4.9 into equation 4.11.

$$u_B(\mathbf{r}) = \frac{i}{4\pi} \iint d^2 r' \int dp \frac{1}{M} \exp[ik_m p(x - x') + ik_m M(z - z')] \times \\ \times f(\mathbf{r}') a_0 \exp(ik_m(p_0 x' + M_0 z')) \quad (4.15)$$

The integral over r' can be replaced with the Fourier transform of $f(\mathbf{r}')$.

$$\hat{F}(k_m(\mathbf{s} - \mathbf{s}_0)) = \frac{1}{2\pi} \iint d^2 r' f(\mathbf{r}') \exp(-ik_m(\mathbf{s} - \mathbf{s}_0)\mathbf{r}') \quad (4.16)$$

The equation for the Born approximation now reads

$$u_B(\mathbf{r}) = \frac{ia_0}{4\pi} \int dp \frac{2\pi}{M} \hat{F}(k_m(\mathbf{s} - \mathbf{s}_0)) \exp(ik_m \mathbf{s} \mathbf{r}). \quad (4.17)$$

We measure the field at the detector line $\mathbf{r} \rightarrow \mathbf{r}_D = (x_D, l_D)$ and at the angle ϕ_0 . Here, l_D is the distance of the detector plane from the rotational center of the sample.

$$u_{B,\phi_0}(\mathbf{r}_D) = \frac{ia_0}{2} \int dp \frac{1}{M} \hat{F}(k_m(\mathbf{s} - \mathbf{s}_0)) \exp(ik_m \mathbf{s} \mathbf{r}_D) \quad (4.18)$$

The subscript ϕ_0 denotes the angular position of the sample and the direction of the incoming plane wave with respect to the sample. In order to arrive at the Fourier diffraction theorem in two dimensions, we perform a one-dimensional Fourier transform of $u_B(\mathbf{r}_D)$ along x_D .

$$\hat{U}_{B,\phi_0}(k_{Dx}) = \frac{ia_0}{2\sqrt{2\pi}} \int dx_D \int dp \frac{1}{M} \hat{F}(k_m(\mathbf{s} - \mathbf{s}_0)) \exp(ik_m(px_D + Ml_D)) \times \\ \times \exp(-ik_{Dx}x_D) \quad (4.19)$$

We now identify the delta distribution

$$\delta(k_{\text{m}}p - k_{\text{Dx}}) = \frac{1}{2\pi} \int dx_{\text{D}} \exp(i(k_{\text{m}}p - k_{\text{Dx}})x_{\text{D}}) \quad (4.20)$$

which in turn we can use to solve the integral over dp .

Note that $\delta(k_{\text{m}}p - k_{\text{Dx}}) = \frac{1}{|k_{\text{m}}|} \delta(p - k_{\text{Dx}}/k_{\text{m}})$.

$$\hat{U}_{\text{B},\phi_0}(k_{\text{Dx}}) = \frac{ia_0 2\pi}{2\sqrt{2\pi}} \int dp \frac{1}{M} \hat{F}(k_{\text{m}}(\mathbf{s} - \mathbf{s}_0)) \exp(ik_{\text{m}}Ml_{\text{D}}) \delta(k_{\text{m}}p - k_{\text{Dx}}) \quad (4.21)$$

Solving the integral implies replacing all occurrences of p with $\frac{k_{\text{Dx}}}{k_{\text{m}}}$.

$$\hat{U}_{\text{B},\phi_0}(k_{\text{Dx}}) = \frac{ia_0\pi}{\sqrt{2\pi}k_{\text{m}}} \frac{1}{\sqrt{1 - \left(\frac{k_{\text{Dx}}}{k_{\text{m}}}\right)^2}} \hat{F}(k_{\text{m}}(\mathbf{s} - \mathbf{s}_0)) \exp\left(ik_{\text{m}}\sqrt{1 - \left(\frac{k_{\text{Dx}}}{k_{\text{m}}}\right)^2} l_{\text{D}}\right) \quad (4.22)$$

Finally, we arrive at the 2D Fourier diffraction theorem

$$\hat{U}_{\text{B},\phi_0}(k_{\text{Dx}}) = \frac{ia_0}{k_{\text{m}}} \sqrt{\frac{\pi}{2}} \frac{1}{M} \hat{F}(k_{\text{m}}(\mathbf{s} - \mathbf{s}_0)) \exp(ik_{\text{m}}Ml_{\text{D}}). \quad (4.23)$$

Note that we have used the substitution $M = \sqrt{1 - \left(\frac{k_{\text{Dx}}}{k_{\text{m}}}\right)^2}$ to simplify the expression. Solving for the Fourier transformed object \hat{F} yields

$$\hat{F}(k_{\text{m}}(\mathbf{s} - \mathbf{s}_0)) = -\sqrt{\frac{2}{\pi}} \frac{ik_{\text{m}}}{a_0} M \hat{U}_{\text{B},\phi_0}(k_{\text{Dx}}) \exp(-ik_{\text{m}}Ml_{\text{D}}). \quad (4.24)$$

The restriction in equation 4.7, rewritten in equation 4.26, forces the one-dimensional Fourier transform of the scattered wave $\hat{U}_{\text{B},\phi_0}(k_{\text{Dx}})$ to be placed on circular arcs in Fourier space:

$$k_{\text{m}}\mathbf{s} = (k_{\text{Dx}} \cos \phi_0 - k_{\text{m}}M \sin \phi_0, k_{\text{Dx}} \sin \phi_0 + k_{\text{m}}M \cos \phi_0) \quad (4.25)$$

$$k_{\text{m}}M = \sqrt{k_{\text{m}}^2 - k_{\text{Dx}}^2} \quad (4.26)$$

The argument $k_{\text{m}}(\mathbf{s} - \mathbf{s}_0)$ shifts the circular arcs in Fourier space such that $\hat{U}_{\text{B},\phi_0}(0)$ is centered at $\hat{F}(0, 0)$.

Comparison to the Fourier Slice Theorem

Equation 4.24 describes the Fourier diffraction theorem in 2D. When compared to the Fourier slice theorem from equation 1.10 in section 1.2, a few differences become apparent. We can write equation 4.24 in the same manner as equation 1.10, with the subscript ϕ_0 denoting the rotation of the object $f(\mathbf{r})$. The main differences are a complex factor and a different distribution of the data in Fourier space, as illustrated in table 4.1.

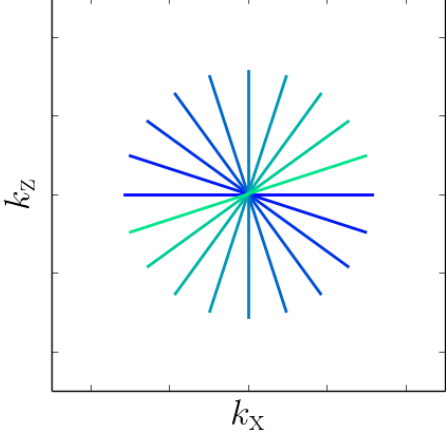
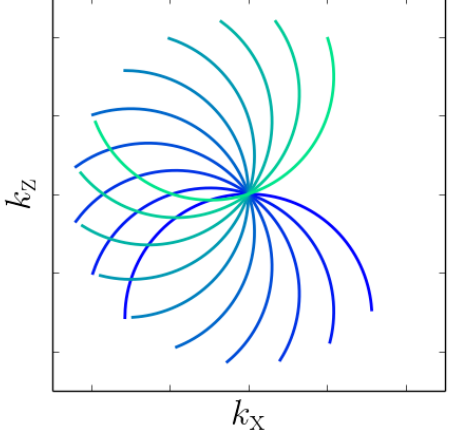
	$\hat{F}_{\phi_0}(k_x, k_z) = A \cdot \sqrt{\frac{1}{2\pi}} \hat{P}_{\phi_0}(k_{Dx})$	
	Fourier Slice Theorem (equation 1.10)	Fourier Diffraction Theorem (equation 4.24)
Sinogram $\hat{P}_{\phi_0}(k_{Dx})$	Fourier transform of projections $\hat{P}_{\phi_0}(k_{Dx})$	Fourier transform of complex scattered waves $\hat{U}_{B,\phi_0}(k_{Dx})$
Factor A	$A = 1$	$A = -\frac{2ik_m M}{a_0} \exp(-ik_m M l_D)$
Coordinates (k_x, k_z) sliced at ϕ_0	$k_x = k_{Dx}$ $k_z = k_t = 0$ (straight line)	$k_x = k_{Dx}$ $k_z = \sqrt{k_m^2 - k_{Dx}^2} - k_m$ (semicircular arc)
Fourier space $\hat{F}(\mathbf{k})$ coverage (180°)		

Table 4.1, Classical versus diffraction tomography. The equation above the table combines the Fourier slice theorem and the Fourier diffraction theorem, pointing out their common structure. However, there are two major differences between the theorems. **(1)** Diffraction tomography data are multiplied by a complex factor $A \neq 1$. **(2)** For diffraction tomography, the Fourier transform of the obtained data is distributed along circular arcs (not straight lines) in Fourier space. The plots show a visualization in Fourier space for data that are sampled at a frequency of $1/k_m$ for angles between 0° and 180° .

4.2. Backpropagation Algorithm

The term *backpropagation* comes from an interpretation of the mathematical formalism which is similar to the backprojection formula derived in section 1.3. The backpropagation algorithm [4] is a solution to the inverse scattering problem. The reconstructed object function $f(\mathbf{r})$ is directly computed from the input data $\hat{U}_B(\mathbf{k})$. For this, we need to perform a coordinate transform from (k_x, k_z) to (k_{Dx}, ϕ_0) . We start by computing the inverse two-dimensional Fourier transform of equation 4.24.

$$\hat{F}(k_m(\mathbf{s} - \mathbf{s}_0)) = -\sqrt{\frac{2}{\pi}} \frac{ik_m}{a_0} M \hat{U}_{B, \phi_0}(k_{Dx}) \exp(-ik_m M l_D) \quad (4.24)$$

$$f(\mathbf{r}) = -\sqrt{\frac{2}{\pi}} \frac{ik_m}{2a_0\pi} \iint dk_x dk_z M \hat{U}_{B, \phi_0}(k_{Dx}) \exp(-ik_m M l_D) \times \exp(ik_m(\mathbf{s} - \mathbf{s}_0)\mathbf{r}) \quad (4.27)$$

$$(k_x, k_z) = k_m(\mathbf{s} - \mathbf{s}_0) \quad (4.28)$$

As described in table 4.1, the input data are distributed along circular arcs in Fourier space. The orientation of these arcs is defined by the acquisition angle ϕ_0 and is described by D_{ϕ_0} .

$$D_{\phi_0} = \begin{pmatrix} \cos \phi_0 & -\sin \phi_0 \\ \sin \phi_0 & \cos \phi_0 \end{pmatrix} \quad (4.29)$$

$$\mathbf{k} = D_{\phi_0} \mathbf{k}' \quad (4.30)$$

Here, \mathbf{k} denotes the non-rotated Fourier space, whereas \mathbf{k}' denotes the positions of acquisition at a certain angle ϕ_0 . At $\phi_0 = 0$, \mathbf{k} and \mathbf{k}' coincide. We have defined the angle ϕ_0 such that, $k'_x = k_{Dx}$ and therefore $k'_z = \sqrt{k_m^2 - k_{Dx}^2} - k_m$. The coordinate transform from (k_x, k_z) to (k_{Dx}, ϕ_0) is now fully described.

$$k_x = k_{Dx} \cos \phi_0 - \left[\sqrt{k_m^2 - k_{Dx}^2} - k_m \right] \sin \phi_0 \quad (4.31)$$

$$k_z = k_{Dx} \sin \phi_0 + \left[\sqrt{k_m^2 - k_{Dx}^2} - k_m \right] \cos \phi_0 \quad (4.32)$$

In order to replace the integrals over k_x and k_z with the integrals over k_{Dx} and ϕ_0 , we compute the Jacobian matrix J and its determinant.

$$J = \frac{\partial k_x \partial k_z}{\partial k_{Dx} \partial \phi_0} \quad (4.33)$$

$$= \begin{pmatrix} \cos \phi_0 + \frac{k_{Dx}}{\sqrt{k_m^2 - k_{Dx}^2}} \sin \phi_0 & -k_{Dx} \sin \phi_0 - \left[\sqrt{k_m^2 - k_{Dx}^2} - k_m \right] \cos \phi_0 \\ \sin \phi_0 - \frac{k_{Dx}}{\sqrt{k_m^2 - k_{Dx}^2}} \cos \phi_0 & k_{Dx} \cos \phi_0 - \left[\sqrt{k_m^2 - k_{Dx}^2} - k_m \right] \sin \phi_0 \end{pmatrix} \quad (4.34)$$

The determinant of the Jacobian J computes to

$$\det(J) = k_{\text{Dx}} - \left(k_{\text{Dx}} - \frac{k_{\text{m}} k_{\text{Dx}}}{\sqrt{k_{\text{m}}^2 - k_{\text{Dx}}^2}} \right) \quad (4.35)$$

$$= \frac{k_{\text{m}} k_{\text{Dx}}}{\sqrt{k_{\text{m}}^2 - k_{\text{Dx}}^2}}. \quad (4.36)$$

We insert the coordinate transform into equation 4.27 and obtain the backpropagation formula.

$$f(\mathbf{r}) = -\sqrt{\frac{2}{\pi}} \frac{i k_{\text{m}}}{2 a_0 \pi} \int dk_{\text{Dx}} \frac{1}{2} \int_0^{2\pi} d\phi_0 \left| \frac{k_{\text{m}} k_{\text{Dx}}}{\sqrt{k_{\text{m}}^2 - k_{\text{Dx}}^2}} \right| M \hat{U}_{\text{B},\phi_0}(k_{\text{Dx}}) \exp(-i k_{\text{m}} M l_{\text{D}}) \times \\ \times \exp(i k_{\text{m}} (\mathbf{s} - \mathbf{s}_0) \mathbf{r}) \quad (4.37)$$

Note that the integration over ϕ_0 goes from 0 to 2π . This is necessary because the Fourier space needs to be covered homogeneously by the projection data. A coverage of only 180° leads to an incomplete coverage in Fourier space as depicted in table 4.1. This aspect is important to keep in mind for later experimental realization. The necessary double-coverage in Fourier space leads to the additional factor $1/2$. Furthermore, we express $(\mathbf{s} - \mathbf{s}_0)$ in terms of a lateral (\mathbf{t}_\perp) and an axial (\mathbf{s}_0) component (eq. 4.31 and 4.32).

$$k_{\text{m}}(\mathbf{s} - \mathbf{s}_0) = k_{\text{Dx}} \mathbf{t}_\perp + k_{\text{m}}(M - 1) \mathbf{s}_0 \quad (4.38)$$

$$\mathbf{s}_0 = (p_0, M_0) = (-\sin \phi_0, \cos \phi_0) \quad (4.39)$$

$$\mathbf{t}_\perp = (-M_0, p_0) = (\cos \phi_0, \sin \phi_0) \quad (4.40)$$

By assuming that $(k_{\text{m}} M)^2 = k_{\text{m}}^2 - k_{\text{Dx}}^2 \stackrel{!}{>} 0$, we can rewrite the backpropagation formula as

$$f(\mathbf{r}) = -\frac{i k_{\text{m}}}{a_0 (2\pi)^{3/2}} \int dk_{\text{Dx}} \int_0^{2\pi} d\phi_0 |k_{\text{Dx}}| \hat{U}_{\text{B},\phi_0}(k_{\text{Dx}}) \exp(-i k_{\text{m}} M l_{\text{D}}) \times \\ \times \exp[i(k_{\text{Dx}} \mathbf{t}_\perp + k_{\text{m}}(M - 1) \mathbf{s}_0) \mathbf{r}]. \quad (4.41)$$

Figure 4.1 illustrates the acquisition and reconstruction process for a non-centered cylinder. The data were computed according to Mie theory. Note that the reconstruction with the Born approximation is not resembling the original structure of the cylinder and that the reconstruction quality with the Rytov approximation is dependent on the total number of projections that were acquired for the sinogram. Also note that the main contribution to the reconstructed refractive index distribution comes from the measured phase. The measured amplitude only slightly influences the reconstruction. Details of the simulation and reconstruction process can be found in figure 4.2.

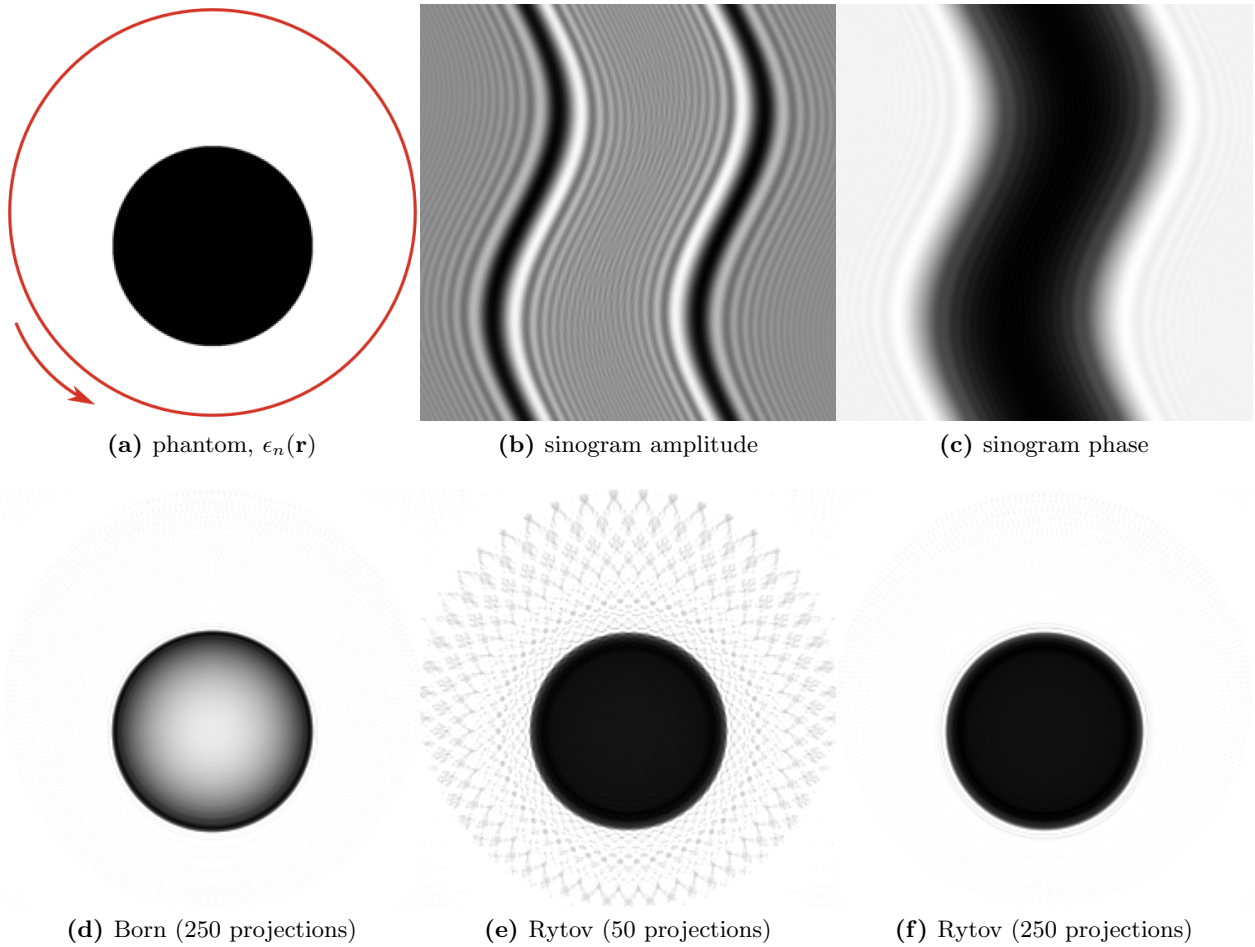


Figure 4.1, 2D Backpropagation. Image (a) shows the refractive index distribution of a dielectric cylinder. White indicates the refractive index of the medium and black the higher refractive index of the cylinder. The forward-scattering process was computed according to Mie theory. Because the cylinder is not centered, the characteristic shape of the sinogram is visible in amplitude (b) and phase (c). The lower images show the reconstruction of the refractive index with (d) the Born approximation using 250 projections, (e) the Rytov approximation using 50 projections, and (f) the Rytov approximation with a total of 250 projections. See figure 4.2 for details.

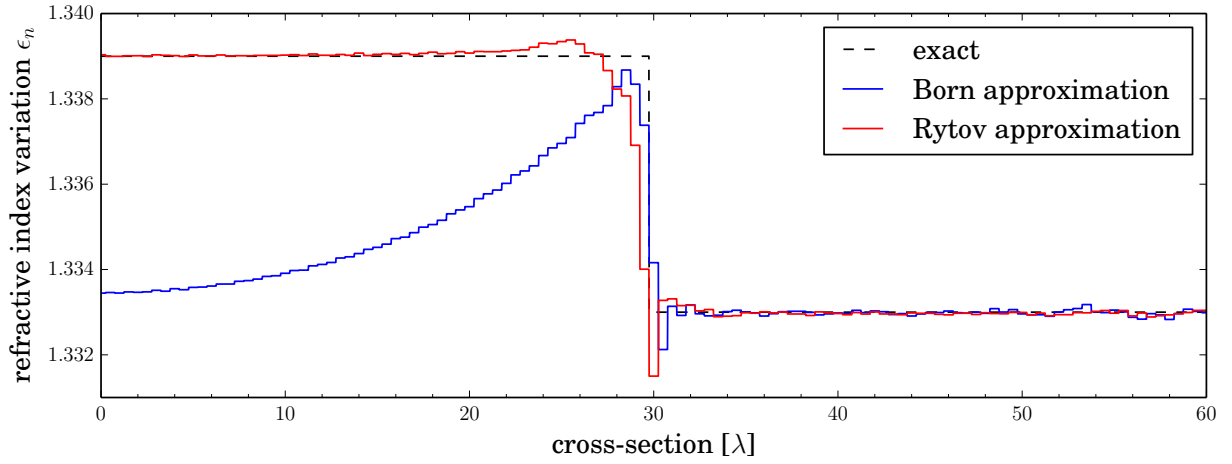


Figure 4.2, 2D Backpropagation cross-sections. The refractive index of the medium is $n_m = 1.333$ and the local variation inside the cylinder is $\epsilon_n(\mathbf{r}) = n(\mathbf{r}) - n_m = 0.006$. The radius of the cylinder is 30λ (vacuum wavelength λ). The scattered wave is computed according to Mie theory at an optical distance of $l_D = 60\lambda$ from the center of the cylinder and sampled at $\lambda/2$ over 250 pixels. The Mie theory computations are based on [20]. The refractive index map is reconstructed on a grid of 250×250 pixels from 250 projections over 2π . The reconstruction was performed with the Python library ODTbrain [21].

Comparison to Backprojection

The main differences between the backprojection and backpropagation algorithms (dependencies on l_D and \mathbf{s}_0) are summarized in table 4.2.

	$f(x, y) = \frac{A}{(2\pi)^{3/2}} \int dk_{Dx} \int_0^{2\pi} d\phi_0 \exp(iB) k_{Dx} \hat{P}_{\phi_0}(k_{Dx})$	
	Backprojection (equation 1.16)	Backpropagation (equation 4.41)
Sinogram $\hat{P}_{\phi_0}(k_{Dx})$	Fourier transform of projections $\hat{P}_{\phi_0}(k_{Dx})$	Fourier transform of complex scattered waves $\hat{U}_{B,\phi_0}(k_{Dx})$
Factor A	$A = \frac{1}{2}$ (double coverage)	$A = -\frac{ik_m}{a_0}$
Exponent B	$B = k_{Dx}(\mathbf{t}_\perp \mathbf{r})$ $\mathbf{t}_\perp = (\cos \phi_0, \sin \phi_0)$	$B = -k_m M l_D + k_{Dx} \mathbf{t}_\perp \mathbf{r} +$ $\quad + k_m (M - 1) \mathbf{s}_0 \mathbf{r}$ $\mathbf{t}_\perp = (\cos \phi_0, \sin \phi_0)$ $\mathbf{s}_0 = (-\sin \phi_0, \cos \phi_0)$

Table 4.2, Backprojection versus backpropagation. The equation above the table illustrates the similar structure of the backprojection and the backpropagation formula. Nevertheless, the backpropagation formula contains an exponent B , resulting from the first Born approximation, that depends on l_D and \mathbf{s}_0 which increases the complexity (See also table 4.1). Note that the backprojection formula has a factor of $1/2$ due to the double coverage over ϕ_0 . The necessity of the 2π -coverage (360°) for the backpropagation algorithm is illustrated by the visualization of the Fourier slice and diffraction theorems in the figures of table 4.1.

5. Three-Dimensional Diffraction Tomography

Two-dimensional (2D) diffraction tomography is valid in three dimensions (3D) only for infinitely elongated objects (i.e. cylinders). For objects that exhibit inhomogeneities along the third dimension, a 3D theory needs to be applied. The 2D and the 3D theory are very similar. There are only a few dimension-specific differences like the position of the Fourier transformed fields along spherical surfaces (3D) instead of circular arcs (2D). This section uses the previous sections as a basis to introduce and discuss the 3D version of diffraction tomography. The notation stays the

same, except that a third axis y is introduced in every vector. As in section 4, we conclude by testing the 3D backpropagation algorithm with data computed according to Mie theory.

5.1. Fourier Diffraction Theorem

There are at least two ways to derive the 3D Fourier diffraction theorem. The first uses a double integral representation of the Green's function. The second makes use of the convolution theorem that connects the convolution of two functions with their product in the Fourier domain. We will thoroughly investigate the first and only briefly discuss the second method.

The Green's function (equation 2.11) of the Helmholtz equation can be rewritten using the double integral representation as shown by Banos et. al⁹ ([22], section 2.11).

$$G(\mathbf{r} - \mathbf{r}') = \frac{ik_m}{8\pi^2} \iint dp dq \frac{1}{M} \exp\{ik_m [p(x - x') + q(y - y') + M(z - z')]\} \quad (5.1)$$

$$M = \sqrt{1 - p^2 - q^2} \quad (5.2)$$

$$\mathbf{s} = (p, q, M) \quad (5.3)$$

Here, we define $k_m \mathbf{s}$ as the wave vector of a plane wave with the wave number k_m . Note that we have introduced the coordinate q in addition to p from the 2D case. In order to keep M real, we now have the restriction $p^2 + q^2 \leq 1$. If this restriction was violated, we would allow evanescent waves which would complicate the inversion process [4]. An incoming plane wave has the normal vector \mathbf{s}_0 that is defined by

$$u_0(\mathbf{r}) = a_0 \exp(ik_m \mathbf{s}_0 \mathbf{r}) \quad (5.4)$$

$$\text{with } \mathbf{s}_0 = (p_0, q_0, M_0). \quad (5.5)$$

In section 3.1 we showed that the Born approximation of $u_s(\mathbf{r})$ reads

$$u_B(\mathbf{r}) = \iiint d^3 r' G(\mathbf{r} - \mathbf{r}') f(\mathbf{r}') u_0(\mathbf{r}'). \quad (5.6)$$

We define the unitary Fourier transform¹⁰ $\hat{F}(\mathbf{k})$ of $f(\mathbf{r})$ in 3D as

$$\hat{F}(\mathbf{k}) = \frac{1}{(2\pi)^{3/2}} \iiint d^3 r f(\mathbf{r}) \exp(-i \mathbf{k} \mathbf{r}) \quad (5.7)$$

$$f(\mathbf{r}) = \frac{1}{(2\pi)^{3/2}} \iiint d^3 k \hat{F}(\mathbf{k}) \exp(i \mathbf{k} \mathbf{r}). \quad (5.8)$$

Furthermore, we define the position of the detector such that its normal vector \mathbf{n}_D is parallel to the incident plane wave vector $k_m \mathbf{s}_0$ ($\mathbf{n}_D = \mathbf{s}_0$). This is a valid assumption, because we only rotate the cell and thus the spatial arrangement of incoming plane wave $u_0(\mathbf{r})$ and detector do not change.

⁹Banos' notation does not include the prefactor $1/(4\pi)$ in the Green's function (see eq 2.11). Therefore, the prefactor in equation 5.1 is $1/(8\pi^2)$ and not $1/(2\pi)$.

¹⁰Please note that other authors, e.g. Devaney [2] may use the non-unitary Fourier transform. The prefactors $(1/(2\pi)^{3/2})$ may differ from our notation.

In the derivations that follow, we make use of the following definition of the Dirac delta function.

$$\delta(x - a) = \frac{1}{2\pi} \int dp \exp(ip(x - a)) \quad (5.9)$$

We insert the definitions of the Green's function and the incident plane wave into the formula for the Born approximation

$$u_B(\mathbf{r}) = \frac{ia_0 k_m}{8\pi^2} \iiint d^3 r' \iint dp dq \frac{1}{M} f(\mathbf{r}') \exp\{-ik_m [(p - p_0)x' + (q - q_0)y' + (M - M_0)z']\} \cdot \exp(ik_m \underbrace{(px + qy + Mz)}_{\mathbf{s}\mathbf{r}}). \quad (5.10)$$

We may interpret the integral over \mathbf{r}' as the Fourier transform of $f(\mathbf{r})$ that is shifted by $-k_m \mathbf{s}_0$ in Fourier space

$$u_B(\mathbf{r}) = \frac{ia_0 k_m}{8\pi^2} (2\pi)^{3/2} \iint dp dq \frac{1}{M} \widehat{F}(\underbrace{k_m(p - p_0), k_m(q - q_0), k_m(M - M_0)}_{k_m(\mathbf{s} - \mathbf{s}_0)}) \cdot \exp(ik_m(px + qy + Mz)). \quad (5.11)$$

Any vector $\mathbf{r}_D = (x_D, y_D, z_D)$ in the detector plane is defined by $\mathbf{n}_D(\mathbf{r} - \mathbf{r}_D) = 0$, where \mathbf{n}_D is the normal vector on the detector plane. We previously placed our detector according to $\mathbf{n}_D = \mathbf{s}_0$, which implies a rotation of the sample perpendicular to the propagation direction \mathbf{s}_0 of the incident plane wave $u_0(\mathbf{r})$. Thus, $z_D = l_D$ is a constant and describes the distance of the detector from the center of the rotation axis. The detected field at the detector plane is thus

$$u_B(\mathbf{r})|_D = u_{B,\phi_0}(\mathbf{r}_D) = \frac{i\pi a_0 k_m}{(2\pi)^{3/2}} \iint dp dq \frac{1}{M} \widehat{F}(k_m(\mathbf{s} - \mathbf{s}_0)) \cdot \exp(ik_m(px_D + qy_D + Ml_D)). \quad (5.12)$$

Now we compute the two-dimensional Fourier transform of the recorded data $u_{B,\phi_0}(\mathbf{r}_D)$ in the detector plane (x_D, y_D) .

$$\widehat{U}_{B,\phi_0}(\mathbf{k}_D) = \frac{i\pi a_0 k_m}{(2\pi)^{5/2}} \iint dx_D dy_D \iint dp dq \frac{1}{M} \widehat{F}(k_m(\mathbf{s} - \mathbf{s}_0)) \cdot \exp(ik_m(px_D + qy_D + Ml_D)) \cdot \exp(-i(k_{Dx}x_D + k_{Dy}y_D)) \quad (5.13)$$

Note that since $k_{Dx}^2 + k_{Dy}^2 + k_{Dz}^2 = k_m^2$, i.e. there is no inelastic scattering, $\widehat{U}_{B,\phi_0}(\mathbf{k}_D)$ must be on a surface of a semi-sphere in Fourier space. When we combine the exponential functions that contain the components of \mathbf{r}_D , we can identify the two-dimensional Dirac delta function

$$\iint dx_D dy_D \exp(ix_D(k_m p - k_{Dx}) + iy_D(k_m q - k_{Dy})) = (2\pi)^2 \delta(k_m p - k_{Dx}, k_m q - k_{Dy}). \quad (5.14)$$

We can now evaluate the integral over p and q .

$$\hat{U}_{B,\phi_0}(\mathbf{k}_D) = \frac{i\pi a_0 k_m}{(2\pi)^{1/2}} \iint dp dq \frac{1}{M} \hat{F}(k_m(\mathbf{s} - \mathbf{s}_0)) \cdot \exp(ik_m M l_D) \cdot \delta(k_m p - k_{Dx}, k_m q - k_{Dy}) \quad (5.15)$$

$$\hat{U}_{B,\phi_0}(\mathbf{k}_D) = \frac{i\pi a_0}{(2\pi)^{1/2} k_m} \iint dp dq \frac{1}{M(p, q)} \hat{F}(k_m [\mathbf{s}(p, q) - \mathbf{s}_0]) \cdot \exp(ik_m M(p, q) l_D) \cdot \delta\left(p - \frac{k_{Dx}}{k_m}, q - \frac{k_{Dy}}{k_m}\right) \quad (5.16)$$

$$\hat{U}_{B,\phi_0}(\mathbf{k}_D) = \frac{i\pi a_0}{(2\pi)^{1/2}} \frac{\exp\left(il_D \sqrt{k_m^2 - k_{Dx}^2 - k_{Dy}^2}\right)}{\sqrt{k_m^2 - k_{Dx}^2 - k_{Dy}^2}} \hat{F}\left(k_{Dx} - k_m p_0, k_{Dy} - k_m q_0, \sqrt{k_m^2 - k_{Dx}^2 - k_{Dy}^2} - k_m \sqrt{1 - p_0^2 - q_0^2}\right) \quad (5.17)$$

We used the identity of the delta function $\delta(Ap) = \frac{1}{|A|} \delta(p)$, and inserted the definition of $M = \sqrt{1 - p^2 - q^2}$ and $\mathbf{s} = (p, q, M)$.

We may write the short form of equation 5.17 by setting

$$k_{Dx} = k_m p \quad \text{and} \quad k_{Dy} = k_m q$$

$$\hat{U}_{B,\phi_0}(\mathbf{k}_D) = \frac{i\pi a_0}{(2\pi)^{1/2}} \frac{\exp(ik_m M l_D)}{k_m M} \hat{F}(\mathbf{k}_D - k_m \mathbf{s}_0) \quad (5.18)$$

When we solve this equation for \hat{F} , we get [3, 4]¹¹

$$\hat{F}(\mathbf{k}_D - k_m \mathbf{s}_0) = \underbrace{-\sqrt{\frac{2}{\pi}} \frac{iMk_m}{a_0} \exp(-ik_m M l_D)}_{\text{complex factor}} \hat{U}_{B,\phi_0}(\mathbf{k}_D). \quad (5.19)$$

5.2. Interpretation of the Fourier Diffraction Theorem

Equation 5.19 shows a direct relation between the Fourier transform of the measured wave (Born approximation) $\hat{U}_{B,\phi_0}(\mathbf{k}_D)$ and the Fourier transform of the inhomogeneity of the sample $\hat{F}(\mathbf{k})$.

5.2.1. Surface of a Semi-Sphere in Fourier Space

A closer look at the arguments reveals that the information defined by $\hat{U}_{B,\phi_0}(\mathbf{k}_D)$ is distributed along a semi-spherical surface with radius k_m in Fourier space that is shifted by $-k_m \mathbf{s}_0$, as is explained in the following.

The spherical surface is defined by the wave vector with the magnitude k_m .

$$k_m^2 = k_{Dx}^2 + k_{Dy}^2 + k_{Dz}^2$$

Because k_{Dx} and k_{Dy} are given by the size of the detector image, we are left with a restriction for k_{Dz} . This restriction forces the data $\hat{U}_{B,\phi_0}(\mathbf{k}_D)$ to be placed on a spherical surface with radius k_m in Fourier space. Thus, the two-dimensional Fourier transform is projected onto a semi-spherical surface as depicted in figure 5.1.

The shift in Fourier space is defined by the argument of $\hat{F}(\mathbf{k}_D - k_m \mathbf{s}_0)$. The information of the Fourier transform of $u_B(\mathbf{r})$ at the detector $\hat{U}_B(\mathbf{k}_D)$ is shifted in Fourier space in the direction $-\mathbf{s}_0$. The vector \mathbf{s}_0 is constant for a fixed value of ϕ_0 and describes the propagation direction of the incident wave onto the sample. The magnitude of the shift is equal to k_m which is the radius of the spherical surface described above.

¹¹If the non-unitary Fourier transform and the sign of the Green's function is taken into account, the term computed by Devaney et al. [3] (equation 48) differs by a factor of $1/(k_m^2)$. This factor k_m^2 comes from a different definition of the data: $f(\mathbf{r}) = -k_m^2 O(\mathbf{r})$ in that paper.

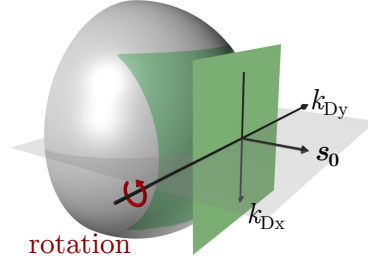


Figure 5.1, Fourier diffraction theorem. The data $\hat{U}_{B,\phi_0}(\mathbf{k}_D)$ (green) are projected onto a semi-sphere in Fourier space according to $k_m^2 = k_{Dx}^2 + k_{Dy}^2 + k_{Dz}^2$. The radius of the sphere is k_m . The surface of the sphere is oriented along the \mathbf{s}_0 axis in the case of coaxial illumination (detector aligned with incoming wave $u_0(\mathbf{r})$). The axes of the two-dimensional Fourier transformed detector image are labeled k_{Dx} and k_{Dy} . If the sample is rotated about one axis (red, here it is the y -axis) and the resolution of the setup is high enough (see sampling considerations below), then one obtains a horn torus-like shape in Fourier space (fig. 5.2).

5.2.2. Sampling Considerations

Diffraction tomography inherently increases and limits the resolution at the same time. As a result of the data distribution on semi-spherical surfaces in Fourier space, the maximum value of $|\mathbf{k}| = |\mathbf{k}_D - k_m \mathbf{s}_0|$ is $\sqrt{2}k_m$. Apparently, the resolution is increased by a factor of $\sqrt{2}$ when compared to the data measured. However, at the same time a maximum possible resolution is enforced by the restriction $|\mathbf{k}| \leq \sqrt{2}k_m$ in Fourier space. For the 2D case, the difference in resolution between projection tomography and diffraction tomography (maximum frequency in Fourier space) is visualized in table 4.1.

It follows that all data distributed in Fourier space are located within a sphere of radius $\sqrt{2}k_m$ according to

$$k_{Dx}^2 + k_{Dy}^2 \leq k_m^2. \quad (5.20)$$

This frequency-limit in Fourier space infers a resolution limit in real space. The maximum frequency in Fourier space computes to

$$f_{\max} = \sqrt{2} \cdot \frac{k_m}{2\pi} = \frac{\sqrt{2}n_m}{\lambda}. \quad (5.21)$$

In other words, the optical resolution is limited to $\lambda/\sqrt{2}n_m$ and depends on the refractive index of the surrounding medium n_m .

5.2.3. Comparison to two-dimensional diffraction tomography

When comparing equations 4.24 and 5.19, it turns out that the Fourier diffraction theorem in two dimensions is similar to the Fourier diffraction theorem in three dimensions. Table 5.1 compares these two equations with respect to their dimensionality.

	$\hat{F}(\mathbf{k}) = A \cdot \sqrt{\frac{1}{2\pi}} \hat{U}_{B,\phi_0}(\mathbf{k}_D)$	
	2D (equation 4.24)	3D (equation 5.19)
Sinogram $\hat{U}_{B,\phi_0}(\mathbf{k}_D)$	Fourier transform of complex scattered waves $\hat{U}_{B,\phi_0}(k_{Dx})$	Fourier transform of complex scattered waves $\hat{U}_{B,\phi_0}(k_{Dx}, k_{Dy})$
Factor A	$A = -\frac{2ik_m M}{a_0} \exp(-ik_m M l_D)$	
	$M = \frac{1}{k_m} \sqrt{k_m^2 - k_{Dx}^2}$	$M = \frac{1}{k_m} \sqrt{k_m^2 - k_{Dx}^2 - k_{Dy}^2}$
Coordinates \mathbf{k} at $\phi_0 = 0$	$\mathbf{k} = (k_x, k_z)$ $k_x = k_{Dx}$ $k_z = \sqrt{k_m^2 - k_{Dx}^2} - k_m$ (semicircular arc)	$\mathbf{k} = (k_x, k_y, k_z)$ $k_x = k_{Dx}, \quad k_y = k_{Dy}$ $k_z = \sqrt{k_m^2 - k_{Dx}^2 - k_{Dy}^2} - k_m$ (semispherical surface)

Table 5.1, Comparison of 2D and 3D diffraction tomography. Above the table is the generalized Fourier diffraction theorem for 2D and 3D. The object $f(\mathbf{r})$ is rotated about the y -axis, which is the axis pointing away from the 2D (x, z) -plane. The shape of the diffraction tomography formula is identical in 2D and in 3D. The only differences come from the different numbers of dimensions. For a comparison to the Fourier slice theorem, see table 4.1.

5.2.4. Artifacts from Uniaxial Rotation

Rotating the sample only about one axis results in missing-angle artifacts for 3D diffraction tomography. According to the Fourier diffraction theorem, the resulting reciprocal volume in Fourier space has a shape similar to a horn torus as depicted in figure 5.2. This implies that the spatial resolution along the axis of rotation (y) is (a) dependent on the x - z position inside the sample and (b) decreases to zero as x and z go to zero. In order to treat these artifacts, regularization techniques need to be applied, as is described in e.g. [23–26].

5.3. The Limes of the Rytov Approximation

In this section we show that diffraction tomography with the Rytov approximation converges to classical tomography when the wavelength λ becomes small [2]. We start with the Fourier diffraction

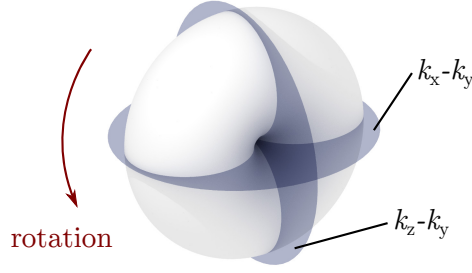


Figure 5.2, Horn torus. As a result of the Fourier diffraction theorem, images acquired perpendicularly to the sample-rotating axis (y) fill a horn torus-like shape in Fourier space. The resulting reconstruction exhibits missing angle artifacts, as shown in figures 5.4 and 5.5

theorem which can be applied in combination with the Rytov approximation by calculating $u_B(\mathbf{r})$ from the measured scattered field $u_s(\mathbf{r}) \approx u_R(\mathbf{r})$ using equation 3.39.

$$u_B(\mathbf{r}) = u_0(\mathbf{r}) \ln \left(\frac{a_0}{a} \left[\frac{u_R(\mathbf{r})}{u_0(\mathbf{r})} + 1 \right] \right) \quad (3.39)$$

$$= u_0(\mathbf{r}) \varphi_R(\mathbf{r}) \quad (3.40)$$

The Fourier transform of the equation above at the detector $\mathbf{r} \rightarrow \mathbf{r}_D$ yields

$$\hat{U}_{B,\phi_0}(\mathbf{k}_D) = \frac{1}{2\pi} \iint d^2 r_D u_0(\mathbf{r}) \varphi_{R,\phi_0}(\mathbf{r}_D) \exp(-i\mathbf{k}_D \mathbf{r}_D) \quad (5.22)$$

$$= \frac{a_0}{2\pi} \iint d^2 r_D \varphi_{R,\phi_0}(\mathbf{r}_D) \exp(-i(\mathbf{k}_D - k_m \mathbf{s}_0) \mathbf{r}_D) \quad (5.23)$$

$$= a_0 \hat{\varphi}_{R,\phi_0}(\mathbf{k}_D - k_m \mathbf{s}_0) \quad (5.24)$$

where $\hat{\varphi}_{R,\phi_0}(\mathbf{k}_D)$ is the two-dimensional Fourier transform of $\varphi_{R,\phi_0}(\mathbf{r}_D)$. For the Rytov approximation, equation 5.19 then reads¹²

$$\hat{F}(\mathbf{k}_D - k_m \mathbf{s}_0) = -\sqrt{\frac{2}{\pi}} i M k_m \exp(-i k_m M l_D) \hat{\varphi}_{R,\phi_0}(\mathbf{k}_D - k_m \mathbf{s}_0). \quad (5.25)$$

By replacing $\mathbf{k}'_D = \mathbf{k}_D - k_m \mathbf{s}_0$ one can rewrite this equation such that the argument of $\hat{F}(\mathbf{k})$ does not anymore contain the shift in Fourier space.

$$\hat{F}(\mathbf{k}'_D) = -\sqrt{\frac{2}{\pi}} i M^* k_m \exp(-i k_m M^* l_D) \hat{\varphi}_{R,\phi_0}(\mathbf{k}'_D) \quad (5.26)$$

$$M^* = \sqrt{1 - (p' + p_0)^2 - (q' + q_0)^2} \quad (5.27)$$

$$\mathbf{k}'_D = k_m(p', q', M') \quad (5.28)$$

$$= k_m(p - p_0, q - q_0, M - M_0) \quad (5.29)$$

¹²Note that \mathbf{k}_D is in a plane as \mathbf{r}_D is defined in the detector plane. Therefore, $\hat{\varphi}_{R,\phi_0}(\mathbf{k}_D - k_m \mathbf{s}_0)$ is a two-dimensional Fourier transform. However, $\hat{F}(\mathbf{k}_D - k_m \mathbf{s}_0)$ is three-dimensional because it contains the k_z component.

The data are still distributed on the surface of a semi-sphere in Fourier space. This information is hidden in the unintuitive restraint from M^*

$$(p' + p_0)^2 + (q' + q_0)^2 \leq 1. \quad (5.30)$$

This expression can be simplified by noting that for $\phi_0 = 0$, \mathbf{k}_D is parallel to \mathbf{s}_0 - our measuring z -direction ($M_0 = 1$) and therefore $p_0 = q_0 = 0$ and

$$p'^2 + q'^2 \leq 1 \quad (5.31)$$

$$M^* = \sqrt{1 - p'^2 - q'^2} \quad (5.32)$$

$$\mathbf{k}'_D = k_m(p, q, M - 1). \quad (5.33)$$

Note that the magnitude of the vector \mathbf{k}'_D is not k_m

$$|\mathbf{k}'_D| = 2k_m(1 - M) \neq k_m \quad (5.34)$$

and thus the restrictions for the k_z component of \mathbf{k}'_D are different. It is shifted by $-k_m$ in the k_z -direction. The shift in Fourier space is not obvious, but it is included in the restrictions for the k_z component of \mathbf{k}'_D .

In the short wavelength limit λ approaches zero and thus k_m , the radius of the semi-spherical surfaces in Fourier space, goes to infinity. The result is a data distribution that is identical to that of the Fourier slice theorem. Furthermore, short wavelengths imply $k_x, k_y \ll k_m$ and we may write $M^* \rightarrow 1$ [2] to obtain

$$\hat{F}(\mathbf{k}'_D) = -\sqrt{\frac{2}{\pi}} i k_m \exp(-i k_m l_D) \hat{\varphi}_{R, \phi_0}(\mathbf{k}'_D) \quad (5.35)$$

$$\hat{\varphi}_{R, \phi_0}(\mathbf{k}'_D) = \frac{1}{2\pi} \iint dx_D dy_D \varphi_{R, \phi_0}(\mathbf{r}_D) \exp(-i \mathbf{k}'_D \mathbf{r}_D) \quad (5.36)$$

$$\hat{F}(\mathbf{k}'_D) = \frac{1}{(2\pi)^{3/2}} \iiint dx dy dz f(\mathbf{r}) \exp(-i \mathbf{k}'_D \mathbf{r}). \quad (5.37)$$

If we perform a two-dimensional Fourier transform of $\hat{F}(\mathbf{k}'_D)$ in the reciprocal detector plane after inserting 5.36 into 5.35, we get a projection along the z -axis smeared out by a periodic exponential.

$$\frac{1}{\sqrt{2\pi}} \int_{-A}^{+A} dz f(\mathbf{r}) = -\sqrt{\frac{2}{\pi}} i k_m \exp(-i k_m l_D) \varphi_{R, \phi_0}(\mathbf{r}_D) \quad (5.38)$$

Where the interval $[-A, A]$ is the domain of $f(\mathbf{r})$ along the z -direction. Here, we used $k_{Dz} = M - 1 \rightarrow 0$. The exponential factor on the right hand side only yields a phase offset in the detector plane. We may set l_D to zero and arrive at [2]

$$\int_{-A}^{+A} dz f(\mathbf{r}) = -2i k_m \varphi_{R, \phi_0}(\mathbf{r}_D). \quad (5.39)$$

The right hand side contains the complex Rytov phase in the detector plane $\varphi_{R,\phi_0}(\mathbf{r}_D) = i\Phi(\mathbf{r}_D)$ (see section 3.2). The left hand side contains the object function from equation 2.9.

$$f(\mathbf{r}) = k_m^2 \left[\left(\frac{n(\mathbf{r})}{n_m} \right)^2 - 1 \right] \quad (2.9)$$

$$= k_m^2 \left[\left(1 + \frac{\epsilon_n(\mathbf{r})}{n_m} \right)^2 - 1 \right] \quad (5.40)$$

$$\epsilon_n(\mathbf{r})^2 \ll \epsilon_n(\mathbf{r}) \approx \frac{2k_m^2}{n_m} \cdot \epsilon_n(\mathbf{r}) \quad (5.41)$$

Where $\epsilon_n(\mathbf{r})$ is the local refractive index variation from the surrounding medium n_m . By writing the right hand side of equation 5.39 as an integral over $d\Phi(\mathbf{r}_D)$, we thus get

$$\int_{-A}^{+A} 2k_m^2 \epsilon_n(\mathbf{r}) \frac{dz}{n_m} = \int 2k_m d\Phi(\mathbf{r}_D) \quad (5.42)$$

$$2k_m^2 \epsilon_n(\mathbf{r}) \frac{dz}{n_m} = 2k_m d\Phi(\mathbf{r}_D) \quad (5.43)$$

$$\frac{\epsilon_n(\mathbf{r})}{\lambda} dz = \frac{1}{2\pi} d\Phi(\mathbf{r}_D). \quad (5.44)$$

This relation describes the phase change $d\Phi$ that occurs over a distance dz , as derived in section 3.1, equation 3.12. Thus, in the limit of high k_m , the Fourier diffraction theorem with the Rytov approximation becomes the Fourier slice theorem, which requires that the data ($\int d\Phi(\mathbf{r}_D)$) recorded at the detector \mathbf{r}_D are computed from line integrals ($\int dz$) through the sample $\epsilon_n(\mathbf{r})$.

5.4. Derivation with the Fourier Transform Approach

An alternative way to derive the Fourier diffraction theorem (equation 5.19) is the convolution approach in Fourier space. This approach uses the convolution theorem for Fourier transforms. We only briefly discuss this approach. For a thorough discussion, see [22].

$$u_B(\mathbf{r}) = \int d^3 r' G(\mathbf{r} - \mathbf{r}') f(\mathbf{r}') u_0(\mathbf{r}') = (G * f u_0)(\mathbf{r}) \quad (5.45)$$

Equation 5.45 describes the Born approximation $u_B(\mathbf{r})$ as a convolution (*) of $G(\mathbf{r})$ with $f(\mathbf{r})u_0(\mathbf{r})$. In Fourier space, we may write $\hat{U}_B(\mathbf{k})$ as¹³

$$\hat{U}_B(\mathbf{k}) = (2\pi)^{3/2} \hat{G}(\mathbf{k}) \cdot \widehat{(f u_0)}(\mathbf{k}), \quad (5.46)$$

where $\widehat{(f u_0)}(\mathbf{k})$ denotes the Fourier transform of $f(\mathbf{r})u_0(\mathbf{r})$, and $\hat{G}(\mathbf{k})$ is the Fourier transform of $G(\mathbf{r})$. We find that

$$\widehat{(f u_0)}(\mathbf{k}) = \frac{a_0}{(2\pi)^{3/2}} \int d^3 r' f(\mathbf{r}') \exp(-i[\mathbf{k} - k_m \mathbf{s}_0] \cdot \mathbf{r}') = a_0 \hat{F}(\mathbf{k} - k_m \mathbf{s}_0) \quad (5.47)$$

¹³The factor $(2\pi)^{3/2}$ originates from the unitary angular frequency Fourier transform. The non-unitary angular frequency and the unitary ordinary frequency Fourier transforms do not show this factor.

is simply a shifted version of the Fourier transform of the inhomogeneity $f(\mathbf{r})$. In order to find $\hat{G}(\mathbf{k})$, we calculate the Fourier transform of the inhomogeneous Helmholtz equation for the Green's function (equation 2.10).

$$\begin{aligned} \frac{1}{(2\pi)^{3/2}} \int d^3 r' \nabla^2 G(\mathbf{r}') \exp(i\mathbf{k}\mathbf{r}') + \overbrace{\frac{1}{(2\pi)^{3/2}} \int d^3 r' k_m^2 G(\mathbf{r}') \exp(i\mathbf{k}\mathbf{r}')}^{k_m^2 \hat{G}(\mathbf{k})} = \\ = -\frac{1}{(2\pi)^{3/2}} \underbrace{\int d^3 r' \delta(\mathbf{r}') \exp(i\mathbf{k}\mathbf{r}')}_1 \end{aligned} \quad (5.48)$$

Using integration by parts for each Cartesian coordinate and by considering the asymptotic behavior

$$\frac{\exp(ikr)}{4\pi r} \rightarrow \frac{\exp(ik|x|)}{4\pi|x|} \text{ as } |x| \rightarrow \infty \quad (5.49)$$

one can show that the first integral in the equation above becomes [22]

$$\frac{1}{(2\pi)^{3/2}} \int d^3 r' \nabla^2 G(\mathbf{r}') \exp(i\mathbf{k}\mathbf{r}') = -k^2 \hat{G}(\mathbf{k}). \quad (5.50)$$

Thus, we obtain the Fourier transform of the Green's function

$$\hat{G}(\mathbf{k}) = \frac{1}{(2\pi)^{3/2}} \frac{1}{k^2 - k_m^2} = \frac{1}{(2\pi)^{3/2}} \frac{1}{k_x^2 + k_y^2 + k_z^2 - k_m^2}. \quad (5.51)$$

We combine the equations above and obtain

$$\hat{U}_B(\mathbf{k}) = \frac{a_0}{k^2 - k_m^2} \cdot \hat{F}(\mathbf{k} - k_m \mathbf{s}_0). \quad (5.52)$$

This equation looks very much like equation 5.19. However, here the entire field $\hat{U}_B(\mathbf{k})$ is on the left hand side of the equation. Since we measure the field at the detector $\hat{U}_{B,\phi_0}(\mathbf{k}_D)$, we perform an inverse Fourier transform to normal space, then take the field $u_B(\mathbf{r})$ at the detector, and finally back-transform to two-dimensional Fourier space. We rotate our coordinate system such that \mathbf{s}_0 matches the k_z -axis. The integral over dk_z can be evaluated using the residue theorem. We integrate around the singularity at $k_z = \sqrt{k_m^2 - k_x^2 - k_y^2}$.

$$u_B(\mathbf{r}) = \frac{a_0}{(2\pi)^{3/2}} \iiint dk_x dk_y dk_z \frac{\exp(i\mathbf{k}\mathbf{r})}{k^2 - k_m^2} \cdot \hat{F}(\mathbf{k} - k_m \mathbf{s}_0) \quad (5.53)$$

$$= \frac{2\pi i a_0}{(2\pi)^{3/2}} \iint dk_x dk_y \frac{\exp\left(i \left[k_x x + k_y y + \sqrt{k_m^2 - k_x^2 - k_y^2} z \right]\right)}{2\sqrt{k_m^2 - k_x^2 - k_y^2}} \cdot \hat{F}(\mathbf{k} - k_m \mathbf{s}_0) \quad (5.54)$$

Here, we used the following partial fraction expansion to obtain the singularities.

$$\frac{1}{k_z^2 - k_m'^2} = \frac{1}{2k_m'} \left(\frac{1}{k_z - k_m'} - \frac{1}{k_z + k_m'} \right) \quad (5.55)$$

$$k_m'^2 = k_m^2 - k_x^2 - k_y^2 \quad (5.56)$$

We identify \mathbf{k} as $\mathbf{k}_D = (x_D, y_D, z_D = l_D)$ (at $\phi_0 = 0$) and perform the two-dimensional Fourier transform at the detector. We obtain delta functions for x and y that we use to solve the integral for k_x and k_y ¹⁴. With $M = \sqrt{k_m^2 - k_{Dx}^2 - k_{Dy}^2}$ we arrive at equation 5.19.

$$\hat{U}_{B,\phi_0}(\mathbf{k}_D) = 2\pi \frac{ia_0}{(2\pi)^{1/2} \cdot 2} \frac{\exp(ik_m M l_D)}{k_m M} \hat{F}(\mathbf{k}_D - k_m \mathbf{s}_0) \quad (5.57)$$

5.5. Backpropagation Algorithm

In this section we derive the three-dimensional analog to the two-dimensional backpropagation algorithm as described by Devaney [3] and section 4.2 in this script. Our goal is to solve equation 5.19 for $f(\mathbf{r})$ such that we do not need any interpolation in Fourier space. In order to do that, we need to perform a change of coordinates. The coordinate system has its origin on the rotating axis y . We define our new coordinate system in the Fourier domain analogous to the two-dimensional case in three steps.

First, we construct our coordinate system such that we can eliminate any reciprocal distances and express any position of the recorded data in terms of angles. This is possible, because the Fourier diffraction theorem states that every point in Fourier space is placed on a semi-sphere with radius k_m centered at $-k_m \mathbf{s}_0$. Second, we define the projection angle ϕ_0 as the angle that corresponds to the angular sample position from which the projection was recorded. The angle ϕ_0 coincides with the direction of the incoming plane wave \mathbf{s}_0 . Note that ϕ_0 is a two-dimensional angle. However, if the sample is rotated only about one axis, the angle ϕ_0 will become one-dimensional. We only consider the rotation about the y -axis as shown in figure 5.3a. Figure 5.3b depicts the two angles which define the semi-spherical surface in spherical coordinates relative to the rotated coordinate system (ϕ_0). Third, we set the polar angle as θ and the azimuthal angle as ψ . For $\phi_0 = 0$, the non-shifted semi-sphere lies within the half-space $k_z \geq 0$. The polar angle θ is then measured from the positive k_z -axis and the azimuthal angle ψ is measured from the k_x -axis in positive direction of k_y . The corresponding variable domains are

$$\begin{aligned} \theta &\in \left[-\frac{\pi}{2}, +\frac{\pi}{2} \right] \\ \psi &\in [0, \pi]. \end{aligned}$$

Let us first write the rotation matrix D_{ϕ_0} for the rotation of the sample about the y -axis.

$$D_{\phi_0} = \begin{pmatrix} \cos \phi_0 & 0 & -\sin \phi_0 \\ 0 & 1 & 0 \\ \sin \phi_0 & 0 & \cos \phi_0 \end{pmatrix} \quad (5.58)$$

¹⁴Factors: the two-dimensional Fourier transform adds a factor of $1/(2\pi)$ and the delta functions contribute with 2π each.

The matrix D_{ϕ_0} rotates a vector \mathbf{s}' counter-clockwise through the angle ϕ_0 about the k_y -axis. The vector that describes the semi-spherical surface in spherical coordinates is given by

$$\mathbf{s}' = (\sin \theta \cos \psi, \sin \psi \sin \theta, \cos \theta)^\top \quad (5.59)$$

where $()^\top$ denotes the transpose of the vector, i.e. \mathbf{s}' is a column vector. We transform this vector into the rotated coordinate system by calculation of

$$\mathbf{s} = D_{\phi_0} \cdot \mathbf{s}' = \begin{pmatrix} \sin \theta \cos \phi_0 \cos \psi - \sin \phi_0 \cos \theta \\ \sin \psi \sin \theta \\ \sin \phi_0 \sin \theta \cos \psi + \cos \phi_0 \cos \theta \end{pmatrix}. \quad (5.60)$$

We use the change of coordinates in Fourier space to rewrite the inverse Fourier integral for $f(\mathbf{r})$ (eq. 5.19)

$$\hat{F}(\mathbf{k}_D - k_m \mathbf{s}_0) = -\sqrt{\frac{2}{\pi}} \frac{iMk_m}{a_0} \exp(-ik_m M l_D) \hat{U}_B(\mathbf{k}_D) \quad (5.19)$$

$$f(\mathbf{r}) = \frac{1}{(2\pi)^{3/2}} \iiint d^3k \hat{F}(\mathbf{k}) \exp(i\mathbf{k}\mathbf{r}) \quad (5.61)$$

where we used

$$\mathbf{k} = k_m(\mathbf{s} - \mathbf{s}_0) \quad (5.62)$$

$$\mathbf{k}_D = k_m \mathbf{s} \quad (5.63)$$

$$\mathbf{s}_0 = (-\sin \phi_0, 0, \cos \phi_0)^\top. \quad (5.64)$$

The integral over d^3k can be expressed as an integral over ϕ_0 , θ , and ψ by means of the Jacobian matrix J .

$$dk_x dk_y dk_z = |\det(J)| d\phi_0 d\theta d\psi \quad (5.65)$$

$$J = \frac{\partial k_x \partial k_y \partial k_z}{\partial \phi_0 \partial \theta \partial \psi} \quad (5.66)$$

The Jacobian matrix is the matrix of all first-order partial derivatives of the vector

$$\begin{pmatrix} k_x \\ k_y \\ k_z \end{pmatrix} = k_m(\mathbf{s} - \mathbf{s}_0) = k_m \begin{pmatrix} \sin \theta \cos \phi_0 \cos \psi - \sin \phi_0 \cos \theta + \sin \phi_0 \\ \sin \psi \sin \theta \\ \sin \phi_0 \sin \theta \cos \psi + \cos \phi_0 \cos \theta - \cos \phi_0 \end{pmatrix} \quad (5.67)$$

and computes to (column wise):

$$\frac{\partial k_x \partial k_y \partial k_z}{\partial \phi_0} = k_m \begin{pmatrix} -\sin \phi_0 \sin \theta \cos \psi - \cos \phi_0 \cos \theta + \cos \phi_0 \\ 0 \\ \sin \theta \cos \phi_0 \cos \psi - \sin \phi_0 \cos \theta + \sin \phi_0 \end{pmatrix} \quad (5.68)$$

$$\frac{\partial k_x \partial k_y \partial k_z}{\partial \theta} = k_m \begin{pmatrix} \cos \phi_0 \cos \psi \cos \theta + \sin \phi_0 \sin \theta \\ \sin \psi \cos \theta \\ \sin \phi_0 \cos \psi \cos \theta - \sin \theta \cos \phi_0 \end{pmatrix} \quad (5.69)$$

$$\frac{\partial k_x \partial k_y \partial k_z}{\partial \psi} = k_m \begin{pmatrix} -\sin \psi \sin \theta \cos \phi_0 \\ \sin \theta \cos \psi \\ -\sin \phi_0 \sin \psi \sin \theta \end{pmatrix} \quad (5.70)$$

For the integration by substitution we thus need to consider the following factor for the integral¹⁵

$$|\det(J)| = |-k_m^3 (\sin \theta)^2 \cos \psi| \quad (5.71)$$

and we may rewrite the integral for $f(\mathbf{r})$ as

$$f(\mathbf{r}) = \frac{1}{2} \frac{1}{(2\pi)^{3/2}} \int_0^{2\pi} d\phi_0 \int_0^\pi d\theta \int_{-\pi/2}^{+\pi/2} d\psi k_m^3 |(\sin \theta)^2 \cos \psi| \hat{F}(\mathbf{k}) \exp(i\mathbf{k}\mathbf{r}) \quad (5.72)$$

where we have introduced a factor of $1/2$ to compensate for the double- ϕ_0 coverage in Fourier space as we rotate the semi-sphere about the k_y axis from 0 to 2π . Note that this factor only holds for equidistant coverage over 2π . In other cases, weighting factors need to be introduced for each angle ϕ_0 . We have to perform one more coordinate transform to arrive at an integral over the coordinates k_{Dx} and k_{Dy} . These are the coordinates in Fourier space that correspond to direct Fourier transforms of the two-dimensional recorded images at angles ϕ_0 . This coordinate transform is also depicted in figure 5.3 and reads

$$k_{Dx} = k_m \cos \psi \sin \theta \quad (5.73)$$

$$k_{Dy} = k_m \sin \psi \sin \theta. \quad (5.74)$$

For $\phi_0 = 0$, the k_{Dx} -axis coincides with k_x and the k_{Dy} -axis with k_y . The Jacobian determinant J_D for this coordinate transform at the detector then computes to

$$|\det(J_D)| = \frac{\partial k_{Dx} \partial k_{Dy}}{\partial \theta \partial \psi} \quad (5.75)$$

$$= k_m^2 |\cos \theta \sin \theta| \quad (5.76)$$

$$\theta \in [-\pi/2, +\pi/2] \quad k_m^2 \cos \theta |\sin \theta|. \quad (5.77)$$

¹⁵This determinant can easily be calculated using SAGE (<http://www.sagemath.org/>).

In the second variables change of integral for $f(\mathbf{r})$ we identify $k_m \cos \theta = k_m M$.

$$d\theta d\psi = \frac{1}{k_m^2 \cos \theta |\sin \theta|} dk_{Dx} dk_{Dy} \quad (5.78)$$

$$= \frac{1}{k_m^2 M |\sin \theta|} dk_{Dx} dk_{Dy} \quad (5.79)$$

By applying these transforms, one obtains an integral for $f(\mathbf{r})$ over the rotation angle ϕ_0 and the coordinates of the Fourier-transformed image k_{Dx} and k_{Dy} .

$$f(\mathbf{r}) = \frac{1}{2} \frac{1}{(2\pi)^{3/2}} \int_0^{2\pi} d\phi_0 \int_{-k_m}^{k_m} dk_{Dx} \int_{-k_m}^{k_m} dk_{Dy} \frac{|k_{Dx}|}{M} \hat{F}(\mathbf{k}) \exp(i\mathbf{k}\mathbf{r}) \quad (5.80)$$

The k_{Dz} -component of the vector \mathbf{k}_D can be expressed by k_{Dx} , k_{Dy} , and ϕ_0 . We express \mathbf{k} in terms of \mathbf{k}_D and \mathbf{s}_0 , which can be separated into lateral (\mathbf{t}_\perp) and axial (\mathbf{s}_0) components.

$$\mathbf{k} = \mathbf{k}_D - k_m \mathbf{s}_0 = k_m (\mathbf{s} - \mathbf{s}_0) \quad (5.81)$$

$$= k_{Dx} \mathbf{t}_\perp + k_m (M - 1) \mathbf{s}_0 \quad (5.82)$$

$$\mathbf{t}_\perp = \left(\cos \phi_0, \frac{k_{Dy}}{k_{Dx}}, \sin \phi_0 \right)^\top \quad (5.83)$$

$$\mathbf{s}_0 = (-\sin \phi_0, 0, \cos \phi_0)^\top \quad (5.84)$$

$$\mathbf{s}_0 \cdot \mathbf{t}_\perp = 0 \quad (5.85)$$

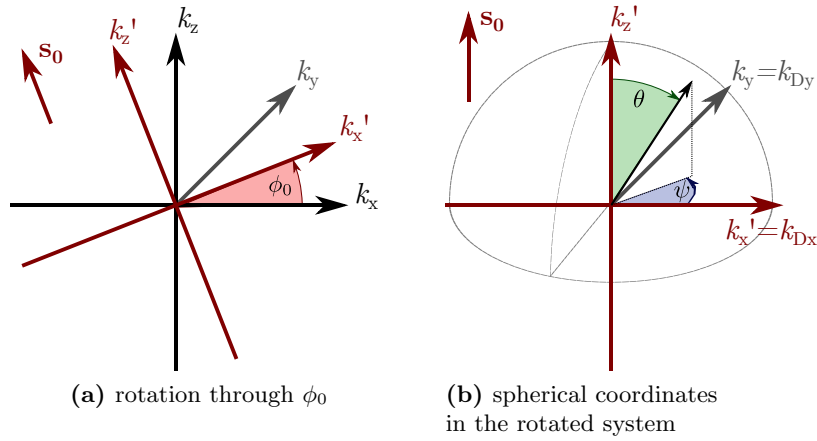


Figure 5.3, Coordinate transforms for 3D backpropagation. **a)** The coordinate system of the detector (red) is rotated about the y -axis which corresponds to a rotation about the k_y -axis in Fourier space. **b)** The position on the semi-spherical surface with the radius k_m is described in a spherical coordinate system with the polar angle θ and the azimuthal angle ψ .

By inserting the relations above, we may express $f(\mathbf{r})$ as

$$f(\mathbf{r}) = \frac{1}{2} \frac{1}{(2\pi)^{3/2}} \int_0^{2\pi} d\phi_0 \int_{-k_m}^{k_m} dk_{Dx} \int_{-k_m}^{k_m} dk_{Dy} \frac{|k_{Dx}|}{M} \widehat{F}(k_{Dx} \mathbf{t}_\perp + k_m(M-1) \mathbf{s}_0) \exp[i(k_{Dx} \mathbf{t}_\perp + k_m(M-1) \mathbf{s}_0) \mathbf{r}]. \quad (5.86)$$

Now we insert equation 5.19. Note that the two-dimensional function $\widehat{U}_{B,\phi_0}(\mathbf{k}_D)$ was measured in the detector plane and thus we write $\widehat{U}_{B,\phi_0}(k_{Dx}, k_{Dy})$. Equation 5.19 describes the Fourier-space distribution of the measurement data from one single projection at an angle ϕ_0 .

$$\widehat{F}(\mathbf{k}_D - k_m \mathbf{s}_0) = -\sqrt{\frac{2}{\pi}} \frac{iMk_m}{a_0} \exp(-ik_m M l_D) \widehat{U}_{B,\phi_0}(k_{Dx}, k_{Dy}) \quad (5.19)$$

The integral over ϕ_0 depends on the recorded data U_{B,ϕ_0} . Furthermore, our choice of coordinates requires the exponential factor in the Fourier transform to be dependent on ϕ_0 .

$$f(\mathbf{r}) = \frac{-ik_m}{(2\pi)^2 a_0} \int_0^{2\pi} d\phi_0 \int_{-k_m}^{k_m} dk_{Dx} \int_{-k_m}^{k_m} dk_{Dy} |k_{Dx}| \widehat{U}_{B,\phi_0}(k_{Dx}, k_{Dy}) \exp(-ik_m M l_D) \exp[i(k_{Dx} \mathbf{t}_\perp + k_m(M-1) \mathbf{s}_0) \mathbf{r}] \quad (5.87)$$

with

$$k_m M = \sqrt{k_m^2 - k_{Dx}^2 - k_{Dy}^2}. \quad (5.88)$$

Equation 5.87 is the three-dimensional backpropagation algorithm of uniaxially rotated samples. An application of the 3D backpropagation algorithm is illustrated in figure 5.4 for a centered sphere from computations that are based on Mie theory. Note that, as could be seen for the 2D case in figure 4.1, the reconstruction with the Born approximation breaks down and that the reconstruction quality with the Rytov approximation is dependent on the total number of projections that were acquired for the sinogram. Details of the simulation and reconstruction process can be found in figure 5.5.

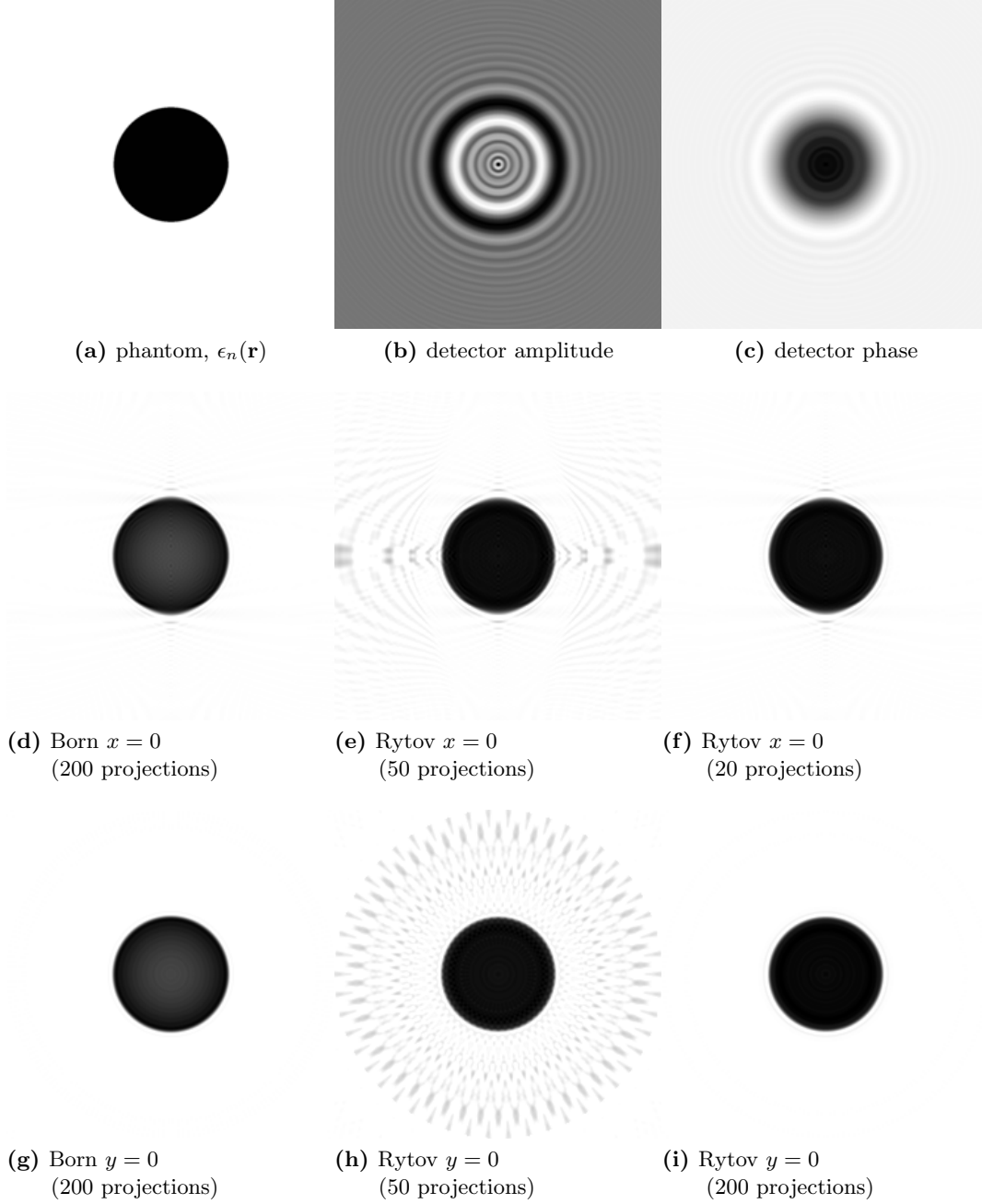


Figure 5.4, 3D Backpropagation. Image (a) shows the refractive index distribution of a dielectric sphere. White indicates the refractive index of the medium and black the higher refractive index of the sphere. The forward-scattering process was computed according to Mie theory. Amplitude and phase of the scattered near-field are shown in (b) and (c). Because the sphere is rotated about its center, the amplitude and phase are identical for every slice of the sinogram. Images (d), (e), and (f) show the reconstruction of the refractive index distribution using the Born and Rytov approximations in the $x = 0$ cross-section. Images (g), (h), and (i) show the corresponding reconstructions at the $y = 0$ cross-section. The reconstruction in (e) and (h) were performed with 50 projections only. See figure 5.5 for details.

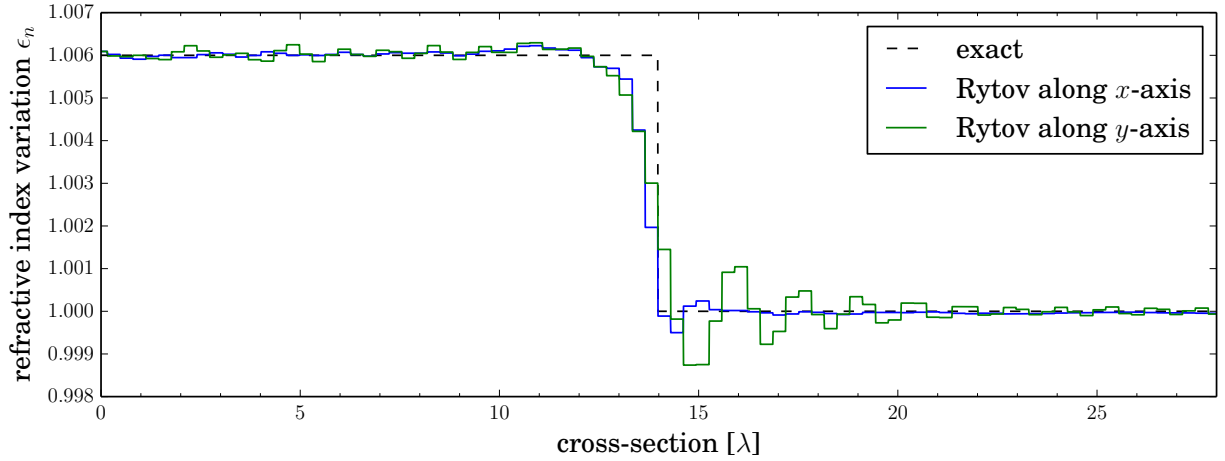


Figure 5.5, 3D Backpropagation cross-sections. The refractive index of the medium is $n_m = 1.0$ and the local variation inside the sphere is $\epsilon_n(\mathbf{r}) = n(\mathbf{r}) - n_m = 0.006$. The radius of the sphere is 14λ (vacuum wavelength λ). The scattered wave is computed at an optical distance of $l_D = 20\lambda$ from the center of the cylinder and sampled at $\lambda/3.1125$ over 250 pixels using the software GMM-FIELD [27]. The refractive index map is reconstructed on a grid of 250×250 pixels from 200 projections over 2π using the software ODTbrain [21]. The reconstruction with the Born approximation (not shown) follows the behavior as seen in figure 4.2. The 2D cross-sections are shown in figure 5.4. Artifacts due to the incomplete 2π -coverage are visible along the y -axis, as briefly discussed in section 5.2.4.

5.5.1. Comparison to the Two-dimensional Backpropagation Algorithm

Table 5.2 summarizes the similarities and differences between the 2D and the 3D backpropagation algorithms with respect to the dimension of the problem.

	$f(\mathbf{r}) = -\frac{ik_m}{2\pi a_0} \left(\int dK_D \right) \int_0^{2\pi} d\phi_0 \exp(iB) k_{Dx} \hat{U}_{B,\phi_0}(\mathbf{k}_D)$	
	2D (equation 4.41)	3D (equation 5.87)
Sinogram $\hat{U}_{B,\phi_0}(\mathbf{k}_D)$	Fourier transform of complex scattered waves $\hat{U}_{B,\phi_0}(k_{Dx})$	Fourier transform of complex scattered waves $\hat{U}_{B,\phi_0}(k_{Dx}, k_{Dy})$
Integral dK_D	$\left(\int dK_D \right) = \frac{1}{\sqrt{2\pi}} \int dk_{Dx}$	$\left(\int dK_D \right) = \frac{1}{2\pi} \iint dk_{Dx} dk_{Dy}$
Exponent B	$B = -k_m M l_D + k_{Dx} \mathbf{t}_\perp \mathbf{r} + k_m (M - 1) \mathbf{s}_0 \mathbf{r}$	
	$M = \frac{1}{k_m} \sqrt{k_m^2 - k_{Dx}^2}$	$M = \frac{1}{k_m} \sqrt{k_m^2 - k_{Dx}^2 - k_{Dy}^2}$
Vectors $\mathbf{r}, \mathbf{s}_0, \mathbf{t}_\perp$	$\mathbf{r} = (x, z)$ $\mathbf{s}_0 = (-\sin \phi_0, \cos \phi_0)$ $\mathbf{t}_\perp = (\cos \phi_0, \sin \phi_0)$	$\mathbf{r} = (x, y, z)$ $\mathbf{s}_0 = (-\sin \phi_0, 0, \cos \phi_0)$ $\mathbf{t}_\perp = \left(\cos \phi_0, \frac{k_{Dy}}{k_{Dx}}, \sin \phi_0 \right)$

Table 5.2, Comparison of 2D and 3D backpropagation. The table compares the 2D and 3D backpropagation algorithms. The generalized backpropagation formula above the table shows that the structure of the algorithms are similar in 2D and 3D, as previously noted in table 5.1. The only differences originate from the different numbers of dimensions. See table 4.2 for a comparison between the backpropagation algorithm and the backprojection algorithm.

6. Implementation

The actual algorithms for backprojection and backpropagation use a trick for the reconstruction. We do not need to numerically integrate the equations for the backprojection (1.16), the two-dimensional (4.41), and the three-dimensional (5.87) backpropagation algorithms. Instead, we identify the Fourier transform for the reciprocal vector \mathbf{k}_D and perform the reconstruction

projection-wise for each rotational position ϕ_0 . In this section, we subsequently derive the actual reconstruction algorithms from the equations of the previous sections.

6.1. Backprojection

The backprojection algorithm, as introduced in section 1, inverts the Radon transform, i.e. it is used to reconstruct an object from equidistant projections. Figure 1.2 depicts the process from image acquisition to image reconstruction with the backprojection algorithm. The backprojection algorithm is based on the Fourier slice theorem [7, 9] and runs as follows:

1. Each projection is filtered with a ramp filter ($|k_{\text{Dx}}|$).
2. The filtered projection is backprojected onto the image volume according to its acquisition angle.
3. The sum of all backprojections constitutes the reconstructed image.

We start from the formula for the inverse Radon transform.

$$f(x, z) = \frac{1}{2\pi} \int dk_{\text{Dx}} \int_0^\pi d\phi_0 |k_{\text{Dx}}| \frac{\hat{P}_{\phi_0}(k_{\text{Dx}})}{\sqrt{2\pi}} \exp[ik_{\text{Dx}}(x \cos \phi_0 + z \sin \phi_0)] \quad (1.16)$$

The data in real space at $\mathbf{r} = (x, y)$ are computed from integrals over k_{Dx} and ϕ_0 . We can introduce a coordinate transform $D_{-\phi_0}$ that rotates \mathbf{r} through the angle $-\phi_0$ along the y -axis, such that $x_{\phi_0} = x \cos \phi_0 + z \sin \phi_0$. In the resulting equation we identify a one-dimensional inverse Fourier transform

$$f(x, z) = \frac{1}{2\pi} \int_0^\pi d\phi_0 D_{-\phi_0} \underbrace{\left\{ \int dk_{\text{Dx}} |k_{\text{Dx}}| \frac{\hat{P}_{\phi_0}(k_{\text{Dx}})}{\sqrt{2\pi}} \exp[ik_{\text{Dx}}x_{\phi_0}] \right\}}_{\text{FFT}_{1\text{D}}^{-1}\{|k_{\text{Dx}}|\hat{P}_{\phi_0}(k_{\text{Dx}})\}} \quad (6.1)$$

We have effectively replaced the integral over k_{Dx} by a one-dimensional inverse fast Fourier transform ($\text{FFT}_{1\text{D}}^{-1}$) and a rotation in real space ($D_{-\phi_0}$). We replace the remaining integral over ϕ_0 by a discrete sum over N equidistant projections and obtain

$$f(x, z) = \frac{1}{2\pi} \sum_{j=1}^N \Delta\phi_0 D_{-\phi_j} \left\{ \text{FFT}_{1\text{D}}^{-1} \left\{ |k_{\text{Dx}}| \hat{P}_{\phi_j}(k_{\text{Dx}}) \right\} \right\} \quad (6.2)$$

with the discrete angular distance $\Delta\phi_0 = \pi/N$ and the discrete angles $\phi_j = j \cdot \Delta\phi_0$ ($j = 1, 2, \dots, N$). A numerical method that implements equation 6.2 is much faster than the direct computation of equation 1.16, because it can make use of the fast Fourier transform. The common name *filtered* backprojection algorithm comes from an interpretation of equation 6.2. The one-dimensional detector data are ramp-filtered and then projected over the entire two-dimensional reconstruction plane according to the angle they were acquired.

A Note on the Ramp Filter

The ramp filter $|k_{\text{Dx}}|$, derived in section 1.3 can also be motivated by the point spread function of the backprojection process, which is $1/|\mathbf{r}|$. By filtering each projection with the ramp filter $|k_{\text{Dx}}|$, the effect of the point spread function can be reversed. To illustrate this, let us consider a reconstructed image that has not been filtered (f_0). Then we may write a formula for the filtered image f by means of the convolution

$$f_0 = f * \frac{1}{|\mathbf{r}|}. \quad (6.3)$$

Inverting this formula using the Fourier transform \mathcal{F} , leads to

$$f_0 = f * \frac{1}{|\mathbf{r}|} = \mathcal{F}^{-1} \left(\underbrace{\mathcal{F}(f) \cdot \mathcal{F}\left(\frac{1}{|\mathbf{r}|}\right)}_{2\pi/|\mathbf{k}|} \right) \quad (6.4)$$

$$f = \mathcal{F}^{-1}(\mathcal{F}(f_0) \cdot |\mathbf{k}|/2\pi) = f * \mathcal{F}^{-1} \left(\underbrace{\mathcal{F}\left(\frac{1}{|\mathbf{r}|}\right) \cdot \frac{|\mathbf{k}|}{2\pi}}_1 \right). \quad (6.5)$$

The derivation shows, that the image in real space f can be computed from the non-filtered backprojection f_0 by multiplication with a two-dimensional ramp filter $|\mathbf{k}|$. Filtering each projection with $|k_{\text{Dx}}|$ is mathematically equivalent and yields better results when working with discrete data sets. With regard to detector symmetries or sample type, other filters (e.g. cosine, Hamming, Hann) have been developed. These filters are usually heuristic and have different effects on image contrast or noise.

6.2. Two-dimensional Backpropagation

The backpropagation algorithm in two dimensions ($\mathbf{r} = (x, z)$) can be derived analogous to the backprojection algorithm. An additional difficulty is introduced by the fact that the projection is now multiplied by a phase factor which is dependent on the distance from the center of the object. Let us consider equation 4.41.

$$f(\mathbf{r}) = -\frac{ik_{\text{m}}}{a_0(2\pi)^{3/2}} \int dk_{\text{Dx}} \int_0^{2\pi} d\phi_0 |k_{\text{Dx}}| \widehat{U}_{\text{B},\phi_0}(k_{\text{Dx}}) \exp(-ik_{\text{m}}Ml_{\text{D}}) \times \exp[i(k_{\text{Dx}} \mathbf{t}_{\perp} + k_{\text{m}}(M-1) \mathbf{s}_0) \cdot \mathbf{r}] \quad (4.41)$$

$$\begin{aligned} \mathbf{t}_{\perp} &= (\cos \phi_0, \sin \phi_0) \\ \mathbf{s}_0 &= (-\sin \phi_0, \cos \phi_0) \end{aligned}$$

We begin by introducing the rotation $D_{-\phi_0}$ through $-\phi_0$ along the y -axis that transforms \mathbf{r} to \mathbf{r}_{ϕ_0} .

$$\mathbf{r}_{\phi_0} = (x_{\phi_0}, z_{\phi_0}) \quad (6.6)$$

$$x_{\phi_0} = x \cos \phi_0 + z \sin \phi_0 \quad (6.7)$$

$$z_{\phi_0} = -x \sin \phi_0 + z \cos \phi_0 \quad (6.8)$$

$$\mathbf{t}_{\perp} \cdot \mathbf{r} = x_{\phi_0} \quad (6.9)$$

$$\mathbf{s}_0 \cdot \mathbf{r} = z_{\phi_0} \quad (6.10)$$

$$\begin{aligned} f(\mathbf{r}) = & -\frac{ik_m}{a_0(2\pi)^{3/2}} \int_0^{2\pi} d\phi_0 \times \\ & \times D_{-\phi_0} \left\{ \int dk_{\text{Dx}} |k_{\text{Dx}}| \widehat{U}_{\text{B},\phi_0}(k_{\text{Dx}}) \exp(-ik_m M l_{\text{D}}) \exp[i(k_{\text{Dx}} x_{\phi_0} + k_m(M-1)z_{\phi_0})] \right\} \end{aligned} \quad (6.11)$$

Because of the factor $k_m(M-1)z_{\phi_0}$ in the integral, we cannot proceed exactly as we did in the previous section. The inverse Fourier transform needs to be performed for all coordinates z_{ϕ_0} before the rotation.

$$\begin{aligned} f(\mathbf{r}) = & -\frac{ik_m}{2\pi \cdot a_0} \int_0^{2\pi} d\phi_0 \times \\ & \times D_{-\phi_0} \left\{ \text{FFT}_{1\text{D}}^{-1} \left\{ |k_{\text{Dx}}| \widehat{U}_{\text{B},\phi_0}(k_{\text{Dx}}) \exp(-ik_m M l_{\text{D}}) \exp[ik_m(M-1)z_{\phi_0}] \right\} \right\} \end{aligned} \quad (6.12)$$

The discretization of the integral over ϕ_0 can be performed according to the previous section

$$\begin{aligned} f(\mathbf{r}) = & -\frac{ik_m}{2\pi \cdot a_0} \sum_{j=1}^N \Delta\phi_0 \times \\ & \times D_{-\phi_j} \left\{ \text{FFT}_{1\text{D}}^{-1} \left\{ |k_{\text{Dx}}| \widehat{U}_{\text{B},\phi_j}(k_{\text{Dx}}) \exp(-ik_m M l_{\text{D}}) \exp[ik_m(M-1)z_{\phi_j}] \right\} \right\} \end{aligned} \quad (6.13)$$

with the discrete angular distance $\Delta\phi_0 = 2\pi/N$ and the discrete angles $\phi_j = j \cdot \Delta\phi_0$ ($j = 1, 2, \dots, N$). When comparing this equation with the backprojection algorithm from equation 6.2, we can see one major difference besides the different filter. The inverse Fourier transform needs to be calculated separately for every distance z_{ϕ_j} . In practice, one first calculates the one-dimensional signal $\widehat{U}_{\text{B},\phi_j}(k_{\text{Dx}}) \exp(-ik_m M l_{\text{D}})$ and then expands the signal by one dimension through the application of the a second filter $\exp[ik_m(M-1)z_{\phi_j}]$. The inverse Fourier transform is then computed along the axis with constant z_{ϕ_j} . The resulting two-dimensional data are rotated by ϕ_j and added to the reconstruction plane. The name “filtered backpropagation” comes from an interpretation of the z_{ϕ_j} -exponential, which looks like a propagation in z_{ϕ_j} -direction.

6.3. Three-dimensional Backpropagation

With the previously described two-dimensional algorithm, it is now straight-forward to derive the three-dimensional analog. We start again from the integral representation.

$$f(\mathbf{r}) = \frac{-ik_m}{(2\pi)^2 a_0} \int_0^{2\pi} d\phi_0 \int_{-k_m}^{k_m} dk_{Dx} \int_{-k_m}^{k_m} dk_{Dy} |k_{Dx}| \times \\ \times \hat{U}_{B,\phi_0}(k_{Dx}, k_{Dy}) \exp(-ik_m M l_D) \exp[i(k_{Dx} \mathbf{t}_\perp + k_m(M-1) \mathbf{s}_0) \mathbf{r}] \quad (5.87)$$

$$\mathbf{t}_\perp = \left(\cos \phi_0, \frac{k_{Dy}}{k_{Dx}}, \sin \phi_0 \right)^\top \\ \mathbf{s}_0 = (-\sin \phi_0, 0, \cos \phi_0)^\top$$

In this section, we only consider the rotation of the sample along the y -axis. This introduces artifacts, as briefly discussed in section 5.2.4. The rotation through $-\phi_0$ is described by the rotation operator $D_{-\phi_0}$ that transforms \mathbf{r}_{ϕ_0} to \mathbf{r} .

$$\mathbf{r} = (x, y, z)^\top \quad (6.14)$$

$$\mathbf{r}_{\phi_0} = (x_{\phi_0}, y_{\phi_0}, z_{\phi_0})^\top \quad (6.15)$$

$$x_{\phi_0} = x \cos \phi_0 + z \sin \phi_0 \quad (6.16)$$

$$y_{\phi_0} = y \quad (6.17)$$

$$z_{\phi_0} = -x \sin \phi_0 + z \cos \phi_0 \quad (6.18)$$

$$\mathbf{t}_\perp \cdot \mathbf{r} = x_{\phi_0} + \frac{k_{Dy}}{k_{Dx}} \cdot y_{\phi_0} \quad (6.19)$$

$$\mathbf{s}_0 \cdot \mathbf{r} = z_{\phi_0} \quad (6.20)$$

$$f(\mathbf{r}) = \frac{-ik_m}{(2\pi)^2 a_0} \int_0^{2\pi} d\phi_0 D_{-\phi_0} \left\{ \int_{-k_m}^{k_m} dk_{Dx} \int_{-k_m}^{k_m} dk_{Dy} |k_{Dx}| \times \right. \\ \left. \times \hat{U}_{B,\phi_0}(k_{Dx}, k_{Dy}) \exp(-ik_m M l_D) \exp[i(k_{Dx} x_{\phi_0} + k_{Dy} y_{\phi_0} + k_m(M-1) z_{\phi_0})] \right\} \quad (6.21)$$

Here, we identify the two-dimensional Fourier transform over k_{Dx} and k_{Dy} and simplify the equation.

$$f(\mathbf{r}) = \frac{-ik_m}{2\pi \cdot a_0} \int_0^{2\pi} d\phi_0 \times \\ \times D_{-\phi_0} \left\{ \text{FFT}_{2D}^{-1} \left\{ \hat{U}_{B,\phi_0}(k_{Dx}, k_{Dy}) |k_{Dx}| \exp(-ik_m M l_D) \exp[ik_m(M-1) z_{\phi_0}] \right\} \right\} \quad (6.22)$$

The final step is to discretize the ϕ_0 -integral

$$f(\mathbf{r}) = \frac{-ik_m}{2\pi \cdot a_0} \sum_{j=1}^N \Delta\phi_0 \times \\ \times D_{-\phi_j} \left\{ \text{FFT}_{2D}^{-1} \left\{ \hat{U}_{B,\phi_j}(k_{Dx}, k_{Dy}) |k_{Dx}| \exp(-ik_m M l_D) \exp[ik_m(M-1) z_{\phi_j}] \right\} \right\} \quad (6.23)$$

with the discrete angular distance $\Delta\phi_0 = 2\pi/N$ and the discrete angles $\phi_j = j \cdot \Delta\phi_0$ ($j = 1, 2, \dots, N$). Equation 6.23 and equation 6.13 only differ in the number of dimensions. In the three-dimensional case, the acquired data are two-dimensional projections through the sample. The fast Fourier transform is used again to speed up the computation. The subsequent rotations are performed for three-dimensional volumes which are then added to the reconstruction volume in the sum over ϕ_0 .

Conclusions

This manuscript reviewed the theory of diffraction tomography. We discussed the wave equation with the Born and Rytov approximations. Next, we compared the mathematical formalism of two-dimensional diffraction tomography with the formalism of classical tomography and pointed out the major differences between them. Subsequently, we derived the full three-dimensional equivalent of diffraction tomography and discussed the implications for biological samples. Finally, we gave details on how to implement the backpropagation algorithm in software. This script is intended as a literature review, establishing the mathematical foundations of diffraction tomography with a coherent notation. The reconstruction methods described are applicable not only to optical diffraction tomography but also to ultrasonic diffraction tomography whose underlying principle is the scalar wave equation. In general, diffraction tomography opens new ways for three-dimensional tissue imaging and with growing computational power at hand, will become a feasible and flexible tool in modern imaging.

A. Notations in Literature

A.1. Two-dimensional Diffraction Tomography

Devaney and Slaney derived the Fourier diffraction theorem with a slightly different notation [3, 18]. This section illustrates the main differences in notation and translates between them. Besides different variable names and a differing definition of the object function $f(\mathbf{r})$, the Devaney and Slaney use the non-unitary angular frequency Fourier transform, whereas this script uses the unitary angular frequency Fourier transform. The Fourier diffraction theorem from equation 4.24 reads

$$\hat{F}(k_m(\mathbf{s} - \mathbf{s}_0)) = -\sqrt{\frac{2}{\pi}} \frac{ik_m}{a_0} M \hat{U}_{B, \phi_0}(k_{Dx}) \exp(-ik_m M l_D). \quad (4.24)$$

Using the notation of Slaney, we start with the Fourier transform of the scattered wave ψ_s ([18], eq. (62)¹⁶).

$$\begin{aligned} \int \psi_s(x, y=l) e^{-i\alpha x} dx &= \frac{1}{2\pi} \tilde{\Gamma}(\alpha, l) \\ \tilde{\Gamma}(\alpha', l) &= \int e^{-i\alpha' x} \int \Gamma_1(\alpha, l) e^{i\alpha x} d\alpha dx \end{aligned}$$

Note that Slaney uses the non-unitary angular frequency Fourier transform. With the identity of the delta function

$$\delta(\alpha - \alpha') = \frac{1}{2\pi} \int e^{i(\alpha - \alpha')x} dx$$

we may write

$$\tilde{\Gamma}(\alpha', l) = \int 2\pi \delta(\alpha - \alpha') \Gamma_1(\alpha', l) d\alpha = 2\pi \Gamma_1(\alpha', l).$$

Using equation 60 from [18], we get¹⁷

$$\int \psi_s(x, y=l) e^{-i\alpha x} dx \stackrel{!}{=} \frac{i\tilde{O}(\alpha, \sqrt{k_o^2 - \alpha^2} - k_o)}{2\sqrt{k_o^2 - \alpha^2}} e^{i\sqrt{k_o^2 - \alpha^2}l}. \quad ([18])$$

Note that in Devaney et al. [3], equation (20) is equivalent to the equation above, when replacing \tilde{O} with $-k^2\tilde{O}$ and performing a one-dimensional Fourier transform. Now we perform the following

¹⁶The factor $\frac{1}{2\pi}$ is missing in [18]: The derivation with the convolution theorem does not seem to be correct. Equation (47) in [18] should read $\tilde{\psi}_s(\vec{\Lambda}) = \tilde{G}(\vec{\Lambda}) * \tilde{H}(\vec{\Lambda})$, where $\tilde{H}(\vec{\Lambda})$ is the Fourier transform of $H(\vec{r}) = \{O(\vec{r})\psi_0(\vec{r})\}$. The additional factor of 2π seems to originate from a delta function in equation (50). The full three-dimensional Fourier transform approach is derived in section 5.4.

¹⁷The exclamation mark (!) in this formula points at the sign of equation (60) and (61) in [18], which should be switched. This follows from the path integration described in the paper.

translations to get from Slaney's notation to the notation in this script.

detector position:

$$(x, y = l) \rightarrow (x_D, z_D = l_D)$$

$$l \rightarrow l_D$$

correlating factor:

$$\sqrt{k_o^2 - \alpha^2} \rightarrow k_m M$$

Fourier transformed object:

$$\tilde{O}(\alpha, \sqrt{k_o^2 - \alpha^2} - k_o) \rightarrow 2\pi \hat{F}(k_m(\mathbf{s} - \mathbf{s}_0))$$

(object function defined at [18], eq. (10))

$$\int \psi_s(x, y = l) e^{-i\alpha x} dx \rightarrow \frac{(2\pi)^{1/2}}{a_0} \hat{U}_{B, \phi_0}(k_{Dx})$$

By replacing these things, we get the equivalent to equation 4.24.

$$\frac{(2\pi)^{1/2}}{a_0} \hat{U}_{B, \phi_0}(k_{Dx}) = \frac{2\pi i \hat{F}(k_m(\mathbf{s} - \mathbf{s}_0))}{2k_m M} \exp(ik_m M l_D)$$

The backpropagation formula (equation 4.41) can be translated via the exact same way. Using the previously mentioned publication by Devaney [3] and combining the equations (35), (36) and (29a) therein, the backpropagation formula reads

$$O_{LD}(\mathbf{r}) = \frac{1}{(2\pi)^2} \int_{-\pi}^{\pi} d\phi_0 \int_{-k}^k d\kappa |\kappa| \underbrace{\tilde{\Gamma}_{\phi_0}(\kappa, \omega)}_{\downarrow} e^{i(\kappa\xi + (\gamma-k)(\eta-l_o)}.$$

$$\int_{-\infty}^{\infty} d\xi \underbrace{\Gamma_{\phi_0}(\xi', \omega)}_{\downarrow} e^{-i\kappa\xi'}$$

$$\frac{ie^{-ikl_o}}{kU_o(\omega)} U_{\phi_0}^{(s)}(\xi', \eta = l_o, \omega)$$

By inserting all of these translations we find the Fourier transform $\hat{U}_{\phi_0}^{(s)}(\kappa, \omega)$ of the scattered wave $U_{\phi_0}^{(s)}(\xi, \eta = l_o, \omega)$.

$$O_{LD}(\mathbf{r}) = \frac{1}{(2\pi)^2} \int_{-\pi}^{\pi} d\phi_0 \int_{-k}^k d\kappa |\kappa| \frac{i}{kU_o(\omega)} \underbrace{\int d\xi' U_{\phi_0}^{(s)}(\xi', \eta = l_o, \omega) e^{-i\kappa\xi'} e^{i(\kappa\xi + (\gamma-k)\eta)} e^{-i\gamma l_o}}_{\hat{U}_{\phi_0}^{(s)}(\kappa, \omega)}$$

We now perform the following translations.

variables:

$$l_o \rightarrow l_D$$

$$k \rightarrow k_m$$

$$\gamma \rightarrow k_m M$$

factors (notation):

$$O_{LD}(\mathbf{r}) \rightarrow -\frac{1}{k_m^2} f(\mathbf{r})$$

(sign and factor k_m^2 defined at [3], eq. (12))

$$\hat{U}_{\phi_0}^{(s)}(\kappa, \omega) \rightarrow \sqrt{2\pi} \hat{U}_{B, \phi_0}(k_{Dx})$$

(non-unitary to unitary Fourier transform)

amplitude:

$$U_o(\omega) \rightarrow a_0$$

vectors:

$$\xi \rightarrow \mathbf{t}_\perp$$

$$\eta \rightarrow \mathbf{s}_0$$

We arrive at the previously derived backpropagation formula.

$$f(\mathbf{r}) = -\frac{ik_m}{a_0(2\pi)^{3/2}} \int dk_{Dx} \int_0^{2\pi} d\phi_0 |k_{Dx}| \hat{U}_{B, \phi_0}(k_{Dx}) \exp(-ik_m M l_D) \times \\ \times \exp[i(k_{Dx} \mathbf{t}_\perp + k_m(M-1) \mathbf{s}_0) \mathbf{r}] \quad (4.41)$$

A.2. Three-dimensional Diffraction Tomography

In section A.1 we looked at two notations in literature that describe the two-dimensional case. The three-dimensional case is briefly discussed by e.g. Devaney [3]. We show the equivalence of the notations by performing a Fourier transform of equation 5.18.

$$u_{B,\phi_0}(\mathbf{r}_D) = \iint \frac{dk_{Dx}dk_{Dy}}{2\pi} \exp(i\mathbf{k}_D\mathbf{r}_D) \frac{i\pi a_0}{(2\pi)^{1/2}} \frac{\exp(ik_m M l_D)}{k_m M} \hat{F}(\mathbf{k}_D - k_m \mathbf{s}_0)$$

The following translations have to be performed to translate between the notation of Devaney and ours.

detector position:

$$(x_D, y_D, z_D = l_D) \rightarrow (x, z, y = l_o)$$

$$l_D \rightarrow l_o$$

$$u_{B,\phi_0}(\mathbf{r}_D) \rightarrow U_B^{(s)}(x, y = l_o, z)$$

correlating factors:

$$a_0 \rightarrow U_o(\omega)$$

$$k_m M \rightarrow \gamma$$

Fourier transformed object:

$$\hat{F}(\mathbf{k}_D - k_m \mathbf{s}_0) \rightarrow -\frac{k^2}{(2\pi)^{3/2}} \tilde{O}(K_x, \gamma - k, K_z)$$

(sign and factor k^2 defined at [3], eq. (12))

We then arrive at equation (46) in [3].

$$U_B^{(s)}(x, y = l_o, z) = -i \frac{k^2}{8\pi^2} U_o(\omega) \iint \frac{dK_x dK_z}{\gamma} e^{i\gamma l_o} \tilde{O}(K_x, \gamma - k, K_z) e^{i[K_x x + K_z z]} \quad ([3], \text{equation (46)})$$

Bibliography

- [1] Emil Wolf. “Three-dimensional structure determination of semi-transparent objects from holographic data”. In: *Optics Communications* 1.4 (Sept. 1969), pp. 153–156. ISSN: 00304018. DOI: 10.1016/0030-4018(69)90052-2.
- [2] A J Devaney. “Inverse-scattering theory within the Rytov approximation”. In: *Optics Letters* 6.8 (Aug. 1981), p. 374. ISSN: 0146-9592. DOI: 10.1364/OL.6.000374.
- [3] A J Devaney. “A filtered backpropagation algorithm for diffraction tomography”. In: *Ultrasonic Imaging* 4.4 (1982), pp. 336–350. ISSN: 0161-7346. DOI: 10.1016/0161-7346(82)90017-7.
- [4] Aninash C. Kak and Malcom Slaney. *Principles of Computerized Tomographic Imaging*. Ed. by Robert E. O’Malley. SIAM, 2001, p. 327. ISBN: 089871494X.
- [5] James Sharpe. “Optical Projection Tomography”. In: *Annual Review of Biomedical Engineering* 6.1 (2004), pp. 209–228. DOI: 10.1146/annurev.bioeng.6.040803.140210.
- [6] Johann Radon. *Über die Bestimmung von Funktionen durch ihre Integralwerte längs gewisser Mannigfaltigkeiten*. Tech. rep. Leipzig: Berichte über die Verhandlungen der Königlich-Sächsischen Gesellschaft der Wissenschaften zu Leipzig, 1917, pp. 262–277.
- [7] R N Bracewell. “Strip Integration in Radio Astronomy”. In: *Australian Journal of Physics* 9.2 (Jan. 1956), pp. 198–217. DOI: 10.1071/2FPH560198.
- [8] Russell M Mersereau. “Direct fourier transform techniques in 3-D image reconstruction”. In: *Computers in Biology and Medicine* 6.4 (1976), 247 –IN4. ISSN: 0010-4825. DOI: 10.1016/0010-4825(76)90064-0.
- [9] R A Brooks and G Di Chiro. “Principles of computer assisted tomography (CAT) in radiographic and radioisotopic imaging”. In: *Physics in Medicine and Biology* 21.5 (1976), p. 689.
- [10] R A Crowther, D J DeRosier, and A Klug. “The Reconstruction of a Three-Dimensional Structure from Projections and its Application to Electron Microscopy”. In: *Proceedings of the Royal Society of London. A. Mathematical and Physical Sciences* 317.1530 (1970), pp. 319–340. DOI: 10.1098/rspa.1970.0119.
- [11] G N Ramachandran and A V Lakshminarayanan. “Three-dimensional reconstruction from radiographs and electron micrographs: application of convolutions instead of Fourier transforms”. In: *PNAS* 68.9 (1971), pp. 2236–2240. DOI: 10.1073/pnas.68.9.2236.
- [12] Paul Müller. *radontea: Python algorithms for the inversion of the Radon transform (Version 0.1.6) [Software]*. <https://pypi.python.org/pypi/radontea/>. 2013.
- [13] Joseph W. Goodman. *Introduction to Fourier Optics*. 3rd. Ben Roberts, 2005, p. 491. ISBN: 0974707724.
- [14] Claude Cohen-Tannoudji, Bernard Diu, and Frank Laloe. *Quantum Mechanics (2 vol. set)*. 2 Volume S. Wiley-VCH, 1992. ISBN: 9780471569527.

- [15] Chen-To Tai. *Dyadic Green Functions in Electromagnetic Theory (IEEE Press Series on Electromagnetic Waves)*. 2 Sub. Institute of Electrical & Electronics Engineering, 1994. ISBN: 9780780304499.
- [16] Philip M Morse and Herman Feshback. *methods of Theoretical Physics [2 Volumes Including Part 1: Chapters 1 to 8 and Part 2: Chapters 9 to 13 Complete]*. 1st. McGraw Hill, 1953. ISBN: 9780976202127.
- [17] Bingquan Chen and Jakob J Stamnes. “Validity of Diffraction Tomography Based on the First Born and the First Rytov Approximations”. In: *Appl. Opt.* 37.14 (1998), pp. 2996–3006. DOI: 10.1364/AO.37.002996.
- [18] M Slaney, A.C. Kak, and L.E. Larsen. “Limitations of Imaging with First-Order Diffraction Tomography”. In: *IEEE Transactions on Microwave Theory and Techniques* 32.8 (Aug. 1984), pp. 860–874. ISSN: 0018-9480. DOI: 10.1109/TMTT.1984.1132783.
- [19] Malcolm Graham Slaney. “Imaging with diffraction tomography”. PhD thesis. Purdue University, 1985.
- [20] Guangran Kevin Zhu. *Cylinder scattering, MATLAB Central File Exchange*. Retrieved 2012. 2011.
- [21] Paul Müller, Mirjam Schürmann, and Jochen Guck. “ODTbrain: a Python library for full-view, dense diffraction tomography”. In: *(manuscript in preparation)* (2015).
- [22] Jr. Banos Alfredo. *Dipole Radiation in the Presence of a Conducting Half-Space (International Series of Monographs in Electromagnetic Waves, Volume 9)*. First Edit. Pergamon Press, 1966.
- [23] Yongjin Sung et al. “Optical diffraction tomography for high resolution live cell imaging.” In: *Optics express* 17.1 (Jan. 2009), pp. 266–77. ISSN: 1094-4087. DOI: 10.1364/OE.17.000266.
- [24] I. Aganj et al. “Regularization for Inverting the Radon Transform With Wedge Consideration”. In: *2007 4th IEEE International Symposium on Biomedical Imaging: From Nano to Macro* (2007), pp. 217–220. DOI: 10.1109/ISBI.2007.356827.
- [25] Lihong Ma et al. “Digital holographic microtomography with few angle data-sets”. In: *Journal of Modern Optics* 0.0 (2014), pp. 1–7. DOI: 10.1080/09500340.2014.923539.
- [26] Samuel J LaRoque, Emil Y Sidky, and Xiaochuan Pan. “Accurate image reconstruction from few-view and limited-angle data in diffraction tomography”. In: *J. Opt. Soc. Am. A* 25.7 (July 2008), pp. 1772–1782. DOI: 10.1364/JOSAA.25.001772.
- [27] Moritz Ringler. “Plasmonische Nahfeldresonatoren aus zwei biokonjugierten Goldnanopartikeln”. 2008.

List of Figures and Tables

Figure 1	Tomographic data acquisition	3
Figure 1.1	3D Radon transform	5
Figure 1.2	Backprojection	7
Figure 4.1	2D Backpropagation	22
Figure 4.2	2D Backpropagation cross-sections	23
Figure 5.1	Fourier diffraction theorem	29
Figure 5.2	Horn torus	31
Figure 5.3	Coordinate transforms for 3D backpropagation	39
Figure 5.4	3D Backpropagation	41
Figure 5.5	3D Backpropagation cross-sections	42
Table 4.1	Classical versus diffraction tomography	19
Table 4.2	Backprojection versus backpropagation	24
Table 5.1	Comparison of 2D and 3D diffraction tomography	30
Table 5.2	Comparison of 2D and 3D backpropagation	43

List of Symbols

c_0	speed of light in vacuum.
$\epsilon_n(\mathbf{r})$	local variation of the refractive index, $\epsilon_n(\mathbf{r}) = n(\mathbf{r}) - n_m$.
$f(\mathbf{r})$	three-dimensional distribution to be reconstructed from two-dimensional projections by inverse methods; in optical tomography $f(\mathbf{r})$ is the inhomogeneity of the wave equation and contains the refractive index distribution $n(\mathbf{r})$, $f(\mathbf{r}) = k_m^2 \left[\left(\frac{n(\mathbf{r})}{n_m} \right)^2 - 1 \right]$.
$\hat{F}(\mathbf{k})$	Fourier transform of $f(\mathbf{r})$.
$G(\mathbf{r} - \mathbf{r}')$	Green's function of the Helmholtz equation.
$\hat{G}(\mathbf{k})$	Fourier transform of the Green's function $G(\mathbf{r})$.
$k(\mathbf{r})$	spatial distribution of the wave number, $k(\mathbf{r}) = k_m \frac{n(\mathbf{r})}{n_m}$.
k_m	wave number in the medium surrounding a sample, $k_m = \frac{2\pi n_m}{\lambda}$.
λ	vacuum wavelength of the laser light that is used for image acquisition.
l_D	distance between rotational center and detector plane.
$n(\mathbf{r})$	refractive index distribution inside a sample, $n(\mathbf{r}) = n_m (1 + \epsilon_n(\mathbf{r}))$.
n_m	refractive index of the medium surrounding a sample.
ϕ_0	angle along which a projection of a sample was recorded; in optical tomography the projections are digital holograms.
$\varphi(\mathbf{r})$	complex phase, $\varphi(\mathbf{r}) = i\Phi(\mathbf{r})$, $u(\mathbf{r}) = a \exp(\varphi(\mathbf{r}))$, $\varphi(\mathbf{r}) = \varphi_0(\mathbf{r}) + \varphi_s(\mathbf{r})$.
$\varphi_0(\mathbf{r})$	complex phase of a plane wave, $u_0(\mathbf{r}) = a_0 \exp(\varphi_0(\mathbf{r}))$.
$\varphi_s(\mathbf{r})$	scattering component of a complex phase $\varphi(\mathbf{r})$.

$\varphi_{\mathbf{R}}(\mathbf{r})$	Rytov approximation to $\varphi_{\mathbf{s}}(\mathbf{r})$.
Φ	phase of an optical wave, $\Phi \in [0, 2\pi)$.
$p_{\phi_0}(\mathbf{r}_{\mathbf{D}})$	projection of a sample onto the detector plane.
$\Psi(\mathbf{r}, t)$	time-dependent propagator of a scalar wave.
ψ	azimuthal angle in the coordinate system of a semi-sphere, $\psi \in [-\pi/2, +\pi/2]$.
R_{ϕ_0}	Radon transform along angle ϕ_0 .
\mathbf{s}	normal unit vector of an arbitrary plane wave, direction of propagation (3D), $\mathbf{s} = (p, q, M)$, $p^2 + q^2 + M^2 = 1$.
\mathbf{s}_0	normal unit vector of an incident plane wave, direction of propagation (3D), $\mathbf{s}_0 = (p_0, q_0, M_0)$, $p_0^2 + q_0^2 + M_0^2 = 1$.
θ	polar angle in the coordinate system of a semi-sphere, $\theta \in [0, \pi]$.
$u(\mathbf{r})$	scattered wave, $u(\mathbf{r}) = u_0(\mathbf{r}) + u_{\mathbf{s}}(\mathbf{r})$.
$u_0(\mathbf{r})$	incident plane or spherical (context) wave, solution to the homogeneous Helmholtz equation.
$u_{\mathbf{s}}(\mathbf{r})$	scattering component of a scattered wave $u(\mathbf{r})$.
$u_{\mathbf{B}}(\mathbf{r})$	Born approximation of $u_{\mathbf{s}}(\mathbf{r})$.
$u_{\mathbf{R}}(\mathbf{r})$	Rytov approximation of $u_{\mathbf{s}}(\mathbf{r})$.
$\hat{U}_{\mathbf{B}}(\mathbf{k})$	Fourier transform of $u_{\mathbf{B}}(\mathbf{r})$.
$\hat{U}_{\mathbf{B}, \phi_0}(\mathbf{k}_{\mathbf{D}})$	Fourier transform of $u_{\mathbf{B}}(\mathbf{r}_{\mathbf{D}})$ at the detector $\mathbf{r}_{\mathbf{D}}$, measured at the angle ϕ_0 . This notation requires that the direction of the incoming plane wave and the detector normal are parallel..

Acknowledgements

We are grateful to Moritz Kreysing, Martin Weigert (Max Planck Institute of Molecular Cell Biology and Genetics, Dresden, Germany), and Kevin Chalut (Cavendish Laboratory, University of Cambridge, Cambridge, UK) for many valuable discussions.

This project has received funding from the European Union's Seventh Framework Programme for research, technological development and demonstration under grant agreement no 282060.